CHALMERS
UNIVERSITY OF TECHNOLOGY

# Controlled deposition of gold nanoparticles on polystyrene

## Towards nanoparticle gradients on plastic substrates

Master's thesis in Nanotechnology

FILIP NEDIN

Department of Chemistry and Chemical Engineering
CHALMERS UNIVERSITY OF TECHNOLOGY
Gothenburg, Sweden 2021

MASTER'S THESIS 2021

# Controlled Deposition of Gold Nanoparticles on Polystyrene

Towards Nanoparticle Gradients on Plastic Substrates

FILIP NEDIN


CHALMERS
UNIVERSITY OF TECHNOLOGY

Department of Chemistry and Chemical Engineering
*Division of Applied Chemistry*
CHALMERS UNIVERSITY OF TECHNOLOGY
Gothenburg, Sweden 2021

Controlled Deposition of Gold Nanoparticles on Polystyrene
Towards Nanoparticle Gradients on Plastic Substrates
FILIP NEDIN



In collaboration with Cline Scientific AB

Supervisors:
Johnas Eklöf, Department of Chemistry and Chemical Engineering
Dr. Hanne Evenbratt, Cline Scientific AB

Examiner:
Ass. Prof. Kasper Moth-Poulsen, Department of Chemistry and Chemical Engineering

Master's thesis 2021
Department of Chemistry and Chemical Engineering
Division of Applied Chemistry
Chalmers University of Technology
SE-412 96 Gothenburg
Telephone: +46 (0)31-772 10 00

Controlled Deposition of Gold Nanoparticles on Polystyrene
Towards Nanoparticle Gradients on Plastic Substrates
FILIP NEDIN
Department of Chemistry and Chemical Engineering
Chalmers University of Technology

# ABSTRACT

Gold nanoparticle (AuNP) number density gradients functionalised with (bio)molecules have applications in the study of e.g. stem cell differentiation. Currently, AuNP number density gradients are available on glass substrates, but many cell cultivation studies are performed on plastic substrates, e.g. polystyrene. Therefore, it is of interest to investigate if AuNP number density gradients can be achieved also on polystyrene.

This thesis investigates several methods of depositing AuNPs on polystyrene substrates. The experimental work is limited to uniform AuNP deposition, thus covering a first step towards AuNP gradients on polystyrene substrates. Two different functionalisation paths were tested: silanisation with aminosilane (APDMES, 3-aminopropyldimethylethoxysilane) and coating with poly-l-lysine (PLL). For the silanisation, $O_2$ plasma, UV/$O_3$ treatment and (base) piranha wash were tested as oxidising pre-treatments. For coating with PLL, $O_2$ plasma was tested as pre-treatment for increased surface wettability. AuNP deposition for the different functionalisation methods is determined by scanning electron microscopy (SEM) and the functionalisation methods are evaluated in terms of AuNP number density and range of interparticle dispersion, as determined by spatial descriptive statistics (Ripley's K function). Furthermore, a rudimental extended random sequential adsorption (RSA) computational model is developed for the system.

Of the tested functionalisation methods, silanisation with pre-treatment by UV/$O_3$ exhibited the most promising results with AuNP number density of same order of magnitude as on glass reference samples ($5.73 \cdot 10^{14}$ $m^{-2}$, compared to $2.48 \cdot 10^{15}$ $m^{-2}$ for the glass reference) and similar range of dispersion (75 nm, compared to 40-60 nm for the glass reference). It should, however, be noted that the conclusions are based on few experiments and need to be verified by additional experiments. The computational model seems to capture the basic phenomena of AuNP adsorption but underestimates the AuNP number density and the interparticle potential, or at least the range of the interparticle potential.

Keywords: AuNP, gradient, polystyrene, APDMES, PLL

# ACKNOWLEDGEMENTS

I would like to thank my supervisors Hanne Evenbratt and Johnas Eklöf and my examiner Kasper Moth-Poulsen for excellent support during my master's thesis work. It was truly a pleasure working together to find both the theoretical and experimental approaches necessary for achieving the results in this thesis.

I would also like to thank the other colleagues at Cline Scientific and Kasper Moth-Poulsen research group at Chalmers for welcoming me to the team and for broadening my view on nanotechnology and its applications in life sciences and energy storage.

Filip Nedin
Malmö, February 2021

## ABBREVIATIONS

| | |
|---|---|
| APDMES | 3-Aminopropyldimethylethoxysilane |
| APTES | 3-Aminopropyltriethoxysilane |
| AuNP | Gold Nanoparticles |
| DLVO | Derjaguin, Landau, Verwey, Overbeek (theory) |
| EDL | Electrical Double Layer |
| LSPR | Localised Surface Plasmon Resonance |
| PLL | Poly-L-Lysine |
| PS | Polystyrene |
| RPM | Revolutions Per Minute |
| RSA | Random Sequential Adsorption |
| SCCM | Standard Cubic Centimetres per Minute |
| SEM | Scanning Electron Microscopy |
| UV | Ultraviolet |
| vdW | van der Waal |

## VARIABLES AND CONSTANTS

| | |
|---|---|
| $A$ | Absorbance [-] |
| $A_H$ | Hamaker constant [J] |
| $A_S$ | Surface area [$m^2$] |
| $B_1;B_2$ | Fitting parameters in eq. (1) [-] |
| $C$ | Concentration [$m^{-3}$] |
| $c$ | Molar concentration [M] |
| $D$ | Distance, between particles or surfaces [m] |
| $d$ | Nanoparticle diameter [nm] |

| | |
|---|---|
| $e$ | Elementary charge ($1.602 \cdot 10^{-19}$ C) |
| $I$ | Ionic strength [M] |
| $k_B$ | Boltzmann constant ($1.38064852 \times 10^{-23}$ JK$^{-1}$) |
| $N$ | Number of nanoparticles [-] |
| $N_A$ | Avogadro constant ($6.022\ldots \cdot 10^{23}$ mol$^{-1}$) |
| $P$ | Probability [-] |
| $p$ | Random variable, used in RSA model for AuNP adsorption [-] |
| $R$ | Nanoparticle radius [m] |
| $r$ | Radius of investigation, used in Ripley's K function [nm] (also denoted $t$ [m]) |
| $T$ | Temperature [K] |
| $t$ | Time [s], or the radius of investigation used in Ripley's K function [m] |
| $W$ | Potential energy (particle-substrate: $W_{ps}$, particle-particle: $W_{pp}$) [J] |
| $Z$ | Analogue to Hamaker constant, used for calculating ELD interactions [J] |
| $z$ | Ion charge [-] |
| $\epsilon_0$ | Permittivity of free space ($8.854\ldots \cdot 10^{-12}$ Fm$^{-1}$) |
| $\epsilon_r$ | Dielectric constant [-] |
| $\zeta$ | Zeta potential [V] |
| $\eta$ | Dynamic viscosity [Pas] |
| $\kappa$ | Inverse of Debye length [m$^{-1}$] |
| $\lambda$ | Wavelength [nm], or average particle number density in Ripley's K function [m$^{-2}$] |
| $\Psi$ | Electrostatic potential [V] |

# TABLE OF CONTENTS

# 1 INTRODUCTION

Since the successful isolation of mouse embryonic stem cells in 1981 [1] and human embryonic stem cells in 1998 [2], stem cells have been of great interest for the use in medicine. Much of the interest lies in one of their defining properties: stem cells can differentiate into a variety of specialised cell types. This property, called pluripotency, implies that stem cells could be cultivated and differentiated to a specific cell type and then implanted into the human body to replace dead or damaged cells. Consequently, stem cells have been proposed as regenerative therapy for several diseases, such as diabetes, Parkinson's disease [2, 3], Alzheimer's disease, muscular degenerative disorder and chronic liver and heart failures [3]. Furthermore, regenerative medicine through stem cell therapy could also play an important role when dealing with the ageing world population, improving tissue functionality by replenishing cells at the end of their life spans.

In order to effectively use stem cells as regenerative therapy, the differentiation process has to be controlled. The differentiation process is sensitive to the local microenvironment of the stem cells, but the exact conditions to produce the desired cells are often not exactly understood and are hard to control. In fact, many studies show only a small percentage of correctly differentiated cells in a mixture of cells of varying differentiation stages [4, 5]. If the correctly derived cells are not purified, this mixture of cells leads to poor tissue performance when implanted into a human body. Undifferentiated embryonic stem cells are especially harmful, as they will spontaneously differentiate into several different cell types and form a type of cancer (teratoma) [6].

To study and better control the differentiation process, Cline Scientific AB develops products with controlled local chemical environment, consisting of gold nanoparticles (AuNPs) adsorbed onto glass substrates. By arranging the AuNPs in a number density gradient along the surface and functionalising the AuNPs with (bio)molecules, a concentration gradient of the (bio)molecule is formed [7]. If appropriate molecules are chosen and the gradient spans a relevant concentration range, the stem cells will differentiate differently at different positions along the surface and the impact of the biomolecule concentration on the differentiation process can thus be studied.

However, not all cell cultivation studies are performed on glass substrates. Aside from glass, most cell cultivation equipment is made of polystyrene. Being a hydrophobic polymer, it behaves differently from the glass substrates currently used. Therefore, to be able to create AuNP gradients on polystyrene substrates, one first needs an understanding of how the polystyrene substrate and its functionalisation affects the AuNP deposition process.

## 1.1 AIMS AND OBJECTIVES

The overall goal of this thesis is to increase the understanding of deposition of gold nanoparticles onto polystyrene substrates and, ultimately, to determine whether AuNP number density gradients can be formed on polystyrene substrates. Objectives include:

- Testing different means of functionalising polystyrene substrates to enable the deposition of AuNPs.
- Depositing AuNPs on polystyrene substrates and characterising the results in terms of AuNP number density and interparticle distances.

- Determining which, if any, of the tested functionalisation methods are suitable for creating AuNP gradients of similar density as on glass substrates.
- Building a rudimental computational model to estimate AuNP density and interparticle distances and comparing the model to experimental results.

## 1.2 SCOPE

The work is limited to uniform AuNP deposition and, thus, covers a first step towards AuNP gradients on polystyrene substrates. As will be shown in subsequent chapters, the deposition process depends on several different parameters. Since the main interest of this thesis is the influence of the substrate and its functionalisation on the deposition process, other parameters will be kept the same as in the procedure for the original glass substrates. The number of functionalisation methods are limited to four methods, which were chosen based on their simplicity and practical use in a future gradient product. Furthermore, the characterisation will not comprise the substrates' morphology and the study will not assess the impact on cytocompatibility of proposed functionalisation methods.

# 2 THEORY

This chapter aims to give an overview of the theoretical background necessary to describe and understand the investigated system. The chapter is divided into four different parts: the first two parts describe the properties of AuNPs and substrates, the third part describes the AuNP deposition process and what factors affect it, and the fourth part describe the principles of characterisation methods employed in the project.

## 2.1 GOLD NANOPARTICLES

As previously mentioned, AuNPs exhibit several interesting properties, enabling them to be of use in a wide range of applications. The properties that are of special interest in this thesis are the optical properties, caused by a phenomenon called local surface plasmon resonance, and the surface chemistry of AuNPs, mainly caused by ligands adsorbed to the AuNP surface.

### 2.1.1 LOCALISED SURFACE PLASMON RESONANCE (LSPR)

One characteristic feature of a AuNP solution is its intense colour, which stems from the plasmonic behaviour inherent to all metals; under irradiation of an electromagnetic wave of proper frequency, the electrical field will cause the free conduction electrons of the metal to start oscillating in resonance with the incoming light [8]. For the case of gold, the penetration depth of the electromagnetic wave is less than 50 nm [9], resulting in the oscillation of surface electrons being most significant. Furthermore, because of the small size of gold nanoparticles, the oscillation is confined in a small space, hence localised.

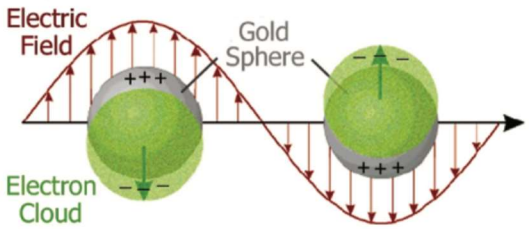


**Figure 1:** Schematic picture of the oscillations of the conduction electrons, caused by an electromagnetic wave **[9]**.

The intense colour of AuNP solutions indicate that they display LSPR peaks in the visible range. The interaction depends on several factors, such as size, morphology and the AuNP's dielectric environment. Focusing on size, it is well known that the absorption peak is blue shifted for decreasing particle size [10, 11, 12], meaning that the solution looks red, and also indicating that the AuNP size could be determined by their optical properties. Using mean free path corrected Mie theory, Haiss, Thanh, Aveyard and Fernig, have shown that the size – and also the concentration – of AuNPs in solution, assuming complete reaction during the AuNP manufacturing process, can be calculated from UV-Vis absorption data alone [13]:

$$d = \exp\left(\frac{B_1 A_{spr}}{A_{450}} - B_2\right) \tag{1}$$

$$c = \frac{A_{450} \cdot 10^{17}}{d^2\left[-0.295 + 1.36\exp\left(-\left(\frac{d-96.8}{78.2}\right)^2\right)\right]} \tag{2}$$

In eq. (1) and (2), $d$ is the particle diameter [nm], $c$ is the nanoparticle concentration [M], $A_{spr}$ and $A_{450}$ are the absorption values at the LSPR peak and at 450 nm, respectively. $B_1$ and $B_2$

are fitting parameters for the functions, determined both theoretically and experimentally to values listed in table 1 below. The theoretical parameter are shown to result in an error in particle size of approximately 18 %, whereas the experimental parameters result in deviations of approximately 11 % [13].

**Table 1:** Parameters used in eq. (1) and (2) **[13]**.

| | **Theoretical value (-)** | **Experimental value (-)** |
|---|---|---|
| $\boldsymbol{B_1}$ | 3.55 | 3.00 |
| $\boldsymbol{B_2}$ | 3.11 | 2.20 |

### 2.1.2 SURFACE CHEMISTRY OF AUNPS

The stability of AuNP solutions and much of the deposition process depend on surface properties, which in turn largely stems from molecules adsorbed onto the surface of the AuNPs.

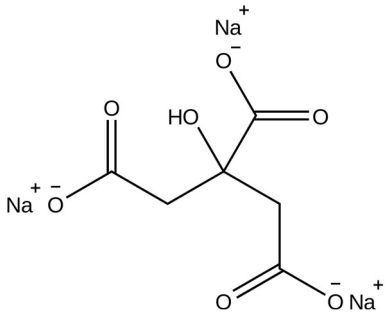


**Figure 2:** Structure of trisodium citrate, $Na_3C_6H_5O_7$, which is a common ligand for AuNPs.

One common ligand, also the ligand used for capping the AuNPs in this project, is citrate, shown in figure 2. It is commonly used in a method of fabricating AuNPs, called the Turkevich method [14] and variations thereof, where it acts as a weak base to reduce the strong acid chloroauric acid, $HAuCl_4$, to form AuNPs. The citrate is then weakly physisorbed onto the gold surface [15], thereby rendering the surface negatively charged and hydrophilic. Several studies suggest different values for the electrostatic potential of citrate stabilised AuNPs, such as -20-25 mV [16], -38.4 ± 2.1 mV [15], -50.6 mV [17], -35.3 mV [11] and -36 mV [18]. Section 2.3.1 will further describe the electrostatic interactions that arise from the citrate layer – both as a stabilising, repulsive force between particles and as a determining factor for AuNP adsorption onto positively charged substrates.

## 2.2 SURFACE CHEMISTRY AND FUNCTIONALISATION OF GLASS AND POLYSTYRENE

Glass is an amorphous solid, mainly consisting of a highly cross-linked silica network ($SiO_2$). At the surface, the network is normally terminated by hydroxyl groups, able to dissociate depending on the pH of the environment. The isoelectric point of glass occurs at approximately pH ≈ 2.1 [19], meaning that the hydroxyl groups dissociate at neutral pH, resulting in the glass surface being negatively charged at neutral pH.

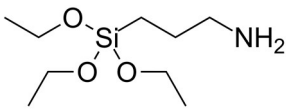


**Figure 3:** Structure of APTES, 3-aminopropyl-triethoxisilane, a commonly used aminosilane for the silanisation of glass.

In order to adsorb negatively charged AuNPs, positive charges can be introduced to the glass surface, for example using silanisation with aminosilanes. A commonly used aminosilane, APTES, is shown in figure 3. The molecule consists of a silicon atom connected to three ethoxy groups, which are hydrolysable, and a group with the desired functionality (amine group, which is positively charged at neutral pH). The silanisation process proceeds in two steps. In the first step, the ethoxy groups are hydrolysed, forming silanols (–Si–OH). In the second step, the silanols react with hydroxyl groups at the glass surface through a condensation reaction, forming siloxane bonds (–Si–O–Si–) with the surface [20].

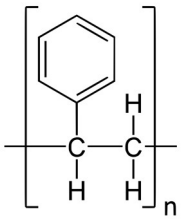


**Figure 4:** Structure of polystyrene.

As evident from figure 4, polystyrene has rather different surface chemistry compared to glass. Polystyrene is too an amorphous material, but is hydrophobic and less reactive than glass, due to the relatively high stability of the phenyl group. Therefore, in order to render a polystyrene surface positively charged, the surface must first be treated by some means. $O_2$ plasma and UV/$O_3$ treatment have been shown to introduce oxygen species at polystyrene surfaces [21]. Specifically, it is proposed that $O_2$ plasma causes ring opening and introduces aldehyde or carboxylate groups, whereas the UV irradiation results in species of lower oxidation states, such as phenol like species [21]. The surface could also be oxidised using Piranha solution (98 % $H_2SO_4$:$H_2O_2$ = 7:3), but the solution is corrosive [22], so it could damage the polystyrene surface, causing undesired surface roughness. Another method, which is applicable to both glass and polystyrene, is coating the surface with a layer of a polymer with a positive charge, e.g. poly-l-lysine (shown below) [23, 24].

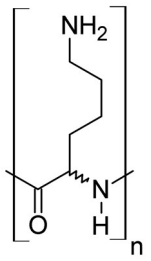


**Figure 5:** Structure of poly-l-lysine.

## 2.3 NANOPARTICLE ADSORPTION

Two theories used for describing nanoparticle adsorption are DLVO theory – describing the forces acting between charged surfaces in a liquid medium – and Random Sequential Adsorption – a stochastic model of the adsorption process.

### 2.3.1 FORCES ACTING BETWEEN CHARGED SURFACES IN A LIQUID MEDIUM

The forces acting between charged surfaces in a liquid medium can be described with the DLVO theory, named after its inventors Derjaguin, Landau, Verwey and Overbeek. It combines the attractive van der Waals forces with the repulsive/attractive interactions of electrical double layers. The repulsive/attractive nature depends on the sign of the surfaces' respective charge. The van der Waals potential between two spheres is described by [25]:

$$W_{vdW}(D) = -\frac{A_H}{6}\left\{\frac{2R_1R_2}{(2R_1+R_2+D)D} + \frac{2R_1R_2}{(2R_1+D)(2R_2+D)} + \ln\frac{(2R_1+2R_2+D)D}{(2R_1+D)(2R_2+D)}\right\} \quad (3)$$

where $A_H$ is the Hamaker constant [J], $R_1$ and $R_2$ are the particle radii [m] and $D$ is the interparticle distance [m]. Between a sphere and a flat surface, a similar expression is derived [25]:

$$W_{vdW}(D) = -\frac{AR}{6D} \quad (4)$$

If the surfaces are charged, there will also be electrostatic interaction between the surfaces, which will be screened by ions present in the liquid medium.

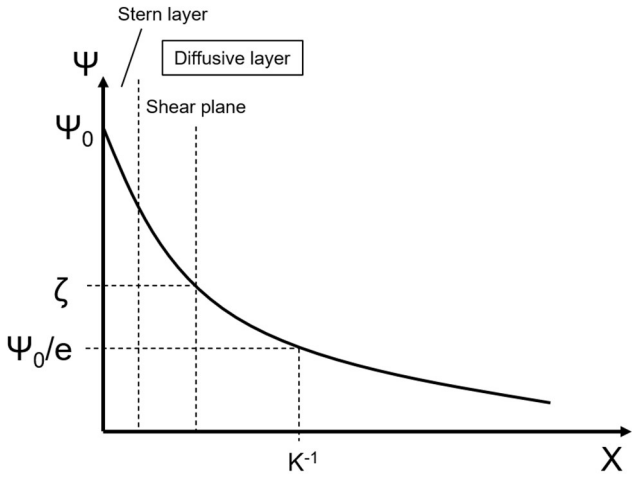


**Figure 6:** Schematic picture of the electrostatic potential **Ψ** at different positions from a charged surface.

Figure 6 shows the electrostatic potential $\Psi$ at some distance $X$ from a charged surface, positioned at $X = 0$, in a liquid medium, As shown, different regions are defined, characterising the local environment near the charged surface. The Stern layer is the innermost layer, where ions of opposite charge to the surface (counter ions) are bound to the surface. Outside the Stern layer – in the diffusive layer – are both counterions and coions with mobility increased by several orders of magnitude compared to in the Stern layer [26]. The two layers together form the electrical double layer (EDL). Furthermore, in the diffusive layer there is a distance where ions can be sheared off (shear plane), and here the zeta potential, $\zeta$, is defined [27]. The Debye length, $\kappa^{-1}$ [m], is the distance where the surface charge, $\Psi_0$, has decreased to $\Psi_0/e$ and it notes the characteristic length of the double layer [26].

For two charged spherical surfaces, the EDL potential can be calculated using [26]:

$$W_{edl}(D) = \left(\frac{R_1 R_2}{R_1 + R_2}\right) Z e^{-\kappa D} \tag{5}$$

where $Z$ is analogous to the Hamaker constant [J], and the Debye length, $\kappa^{-1}$ [m], is defined by:

$$\kappa^{-1} = \sqrt{\frac{\epsilon_r \epsilon_0 k_B T}{2 N_A e^2 I}} \tag{6}$$

where $\epsilon_r$ is the dielectric constant [-], $\epsilon_0$ is the permittivity of free space ($8.854\ldots \cdot 10^{-12}$ $Fm^{-1}$), $k_B$ is the Boltzmann constant ($1.38064852 \cdot 10^{-23}$ $JK^{-1}$), $N_A$ is the Avogadro constant ($6.022\ldots \cdot 10^{23}$ $mol^{-1}$), $e$ is the elementary charge ($1.602 \cdot 10^{-19}$ C) and $I$ is the ionic strength, as defined by:

$$I = \frac{1}{2} \sum c_i z_i^2 \tag{7}$$

where $c_i$ and $z_i$is the concentration and charge of ion $i$ [M]. For a sphere near a surface, the ELD potential is calculated using [26]:

$$W_{edl}(D) = R Z e^{-\kappa D} \tag{8}$$

Eq. (4) and (5) only applies to distances that are larger than the Debye length. Else, the Poisson-Boltzmann equation must be solved by numerical means. An approximation of the total pair potential is achieved by adding the contribution from the van der Waals interactions and the interactions that arise from the electrical double layer:

$$W_{tot}(D) = W_{vdW}(D) + W_{edl}(D) \tag{9}$$

A visualisation of the forces in eq. (9) is presented in figure 7 below.

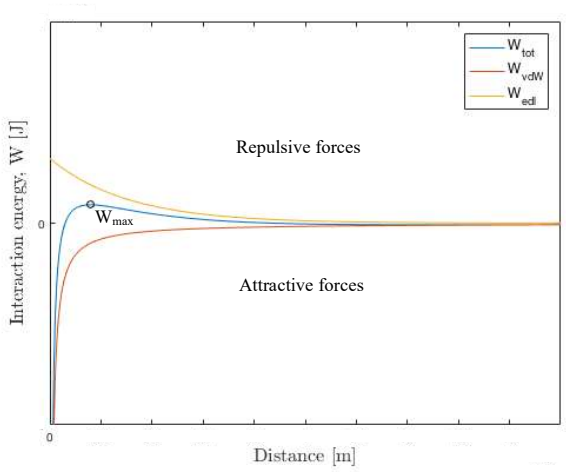


**Figure 7:** A schematic visualisation of the potentials in the DLVO theory. The circle marks the maximum energy barrier, $W_{max}$, that a AuNP has to overcome to either adsorb on a surface or agglomerate with another AuNP.

### 2.3.2 EXTENSIONS TO THE RANDOM SEQUENTIAL ADSORPTION (RSA) MODEL

Random sequential adsorption (RSA) is a model of an irreversible process, during which objects are deposited on a flat surface, e.g. adsorption of proteins on different substrate surfaces. In its standard form, the objects are placed on the surface one after another with coordinates chosen at random, but the objects are not allowed to deposit if overlapping with another object [28]. RSA extended with additional constraints in terms of particle-particle and particle-substrate interactions (according to DLVO theory as presented in section 2.3.1), has been used to model the AuNP adsorption on $Si/SiO_2$ wafers functionalised via silanisation or via coating with poly-l-lysine [24]. In this model, the probability of an AuNP adsorbing to the substrate surface, is given by:

$$P_{ps} = \exp\left(-\frac{W_{ps,max}(D)}{k_B T}\right) \tag{10}$$

where $W_{ps,max}$ is the maximum energy barrier between the AuNP and the substrate, according to DLVO theory (see figure 7) [29]. A similar expression is used to estimate the probability of a AuNP existing at some distance $D$ to another AuNP [24]:

$$P_{pp} = \exp\left(-\frac{W_{pp}(D)}{k_B T}\right) \tag{11}$$

Apart from particle-substrate and particle-particle interactions, the number of AuNPs that adsorb to the substrate surface also depends on the number of AuNPs that diffuse to (the vicinity of) the substrate surface. This is given by:

$$N = A_S C \sqrt{\frac{k_B T t}{12\pi\eta R}} \tag{12}$$

where $N$ is the number of AuNPs [-], $A_S$ is the area at which the diffusion occurs (the substrate surface area) [$m^2$], $C$ is the AuNP concentration [$m^{-3}$], $t$ is the duration of diffusion [s] and $\eta$ is the viscosity of the solvent [Pas] [30].

### 2.3.3 METHODS OF CREATING NANOPARTICLE GRADIENTS

There are several methods for creating AuNP gradients, as the gradient can be achieved in different parts of the AuNP gradient manufacturing process. For example, a gradient of the silanisation can be performed by vapour deposition of silane, during which a silane concentration gradient is formed via the diffusion of silane in the vapour phase [31]. Another alternative – indeed the alternative used as a basis for this thesis – instead involves performing uniform silanisation and gradient deposition of AuNPs.

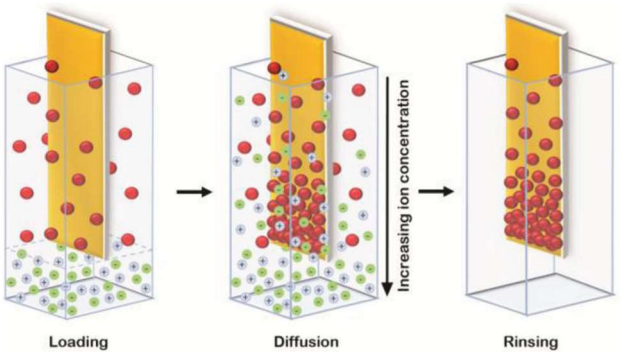


**Figure 8:** Schematic picture of gradient AuNP (red spheres) deposition on a substrate (yellow), using the diffusion of a solution with high ionic strength (green and blue spheres) **[7]**.

As outlined in figure 8, gradient deposition of AuNPs can be achieved by submerging a substrate in a AuNP solution of low ionic strength and loading a solution of high ionic strength at the bottom of the beaker [7]. Since there is a concentration difference between the two solutions, the ions from the solution with high ionic strength will diffuse up the beaker – creating an ionic strength gradient along the substrate surface. Since the repulsive interparticle potential decays with increasing ionic strength, by eq. (5)-(7), the AuNPs at the bottom of the substrate will thus adsorb to the substrate with smaller interparticle distance than the AuNPs at the top of the beaker. Consequently, if the diffusion is stopped (by rinsing the sample) at some time before the solution has reached uniform ion concentration, the resulting AuNP distribution on the substrate surface will be a number density gradient.

## 2.4 SPATIAL DESCRIPTIVE STATISTICS

Spatial descriptive statistics is – as the name implies – the statistical analysis of spatial information, e.g. sets of coordinates (in this thesis the analysis will be employed to coordinates of AuNPs adsorbed onto a substrate). A common area of interest for the spatial analysis focuses on investigating the statistical distribution of the coordinates in terms of dispersion and clustering (see figure 9 below).

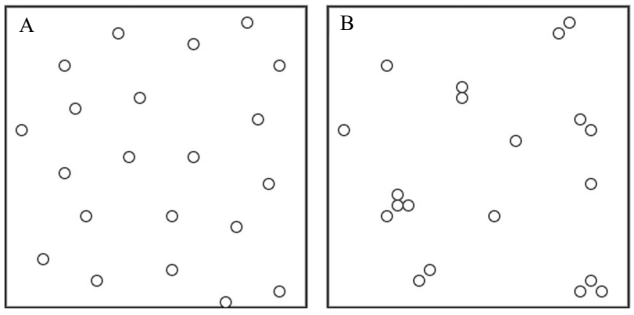


**Figure 9:** Schematic pictures of different types of spatial distributions, showing examples of dispersion (A) and clustering (B).

A numerical representation of the spatial distribution, as exemplified in figure 8, is provided by Ripley's K function [32]:

$$\widehat{K}(t) = \lambda^{-1} \sum_{i=1}^{N_{tot}} \sum_{j \neq i}^{N_{tot}} \frac{I\left(D_{ij} < t\right)}{N_{tot}} \tag{13}$$

For all coordinates (particles), the function investigates circular areas of varying radius $t$. If a particle is found within the radius, $I\left(D_{ij} < t\right)$ is true and 1 is added to the sum [24]. $D_{i,j}$ is the

distance between particles *i* and *j*, $\lambda$ is the average particle number density on the surface and $N$ is the total amount of particles on the sample. For a random Poisson process, $K(t)$ should follow [32]:

$$K(t) = \pi t^2 \tag{14}$$

and by comparing the observed value from eq. (13) with the theoretically expected value from eq. (14), it is possible to obtain information on the spatial distribution of the coordinates; e.g., if $\widehat{K}(t) < K(t)$ for some distance *t*, it follows that fewer particles than expected from the random Poisson process are found and the coordinates are said to be dispersed, and vice versa. Often, the *L* function is used instead of the *K* function, as defined by:

$$L(t) = \sqrt{\frac{K(t)}{\pi}} \tag{15}$$

which should be equal to *t* for a random Poisson process, according to eq. (14). If *L(t)-t* is plotted, a straight line at zero is expected for a random Poisson process. Thus, if the observed value for *L(t)-t* is below (or above) zero, the sample shows dispersion (or clustering).

# 3 EXPERIMENTAL WORK

The experimental work largely consisted of three parts: deposition of AuNPs on glass and polystyrene substrates, characterising the system (e.g. by SEM) and development of a computational model for the AuNP adsorption.

## 3.1 PREPARING GOLD NANOPARTICLE SOLUTIONS

AuNPs were prepared using a modified Turkevich method as described in section 2.1.2. Two solutions were prepared for the nanoparticle synthesis:

**Solution 1**: 32 ml MilliQ water. 8 ml sodium citrate ($Na_3C_6H_5O_7$, 1 % in MilliQ water). 400 µl tannic acid ($C_{76}H_{52}O_{46}$, 1 % in MilliQ water).

**Solution 2**: 160 ml MilliQ water. 160 µl chloroauric acid ($HAuCl_4$, 5 % in MilliQ water)

Both solutions (stirred at 300 RPM) were heated to 60 °C, after which solution 1 was poured into solution 2. The new solution (also stirred at 300 RPM) turned a dark blue colour and after approximately 20 minutes the solution turned red, signalling that AuNPs of the right size (approximately 10 nm) had been formed. The AuNP solution was then heated to 95 °C to complete the reaction, after which the solution (the "batch solution") was either cooled and used directly or stored in refrigerator for later use (more common). Several batch solutions were prepared during the experiments.

When preparing solutions for final use – be it for nanoparticle deposition or characterisation – the batch solution was centrifuged to get concentrated AuNP 'pellets', which could be added to different solutions. Approximately 50 ml of batch solution was transferred to a centrifuge tube (or several 50 ml volumes to several centrifuge tubes, if necessary) and the solution was centrifuged at 11 200 RPM for 1 hour 45 minutes at 4 °C. The centrifuge tubes were carefully removed from the centrifuge, after which about 75 % of the supernatant was removed and 150 µl of AuNP pellet was collected from each centrifuge tube using a micropipette. Looking at the tip when collecting the pellet, it was evident that some part (at least 15 %) of the collected 150 µl volume consisted of supernatant. The collected AuNP pellets were then added to different solutions depending on use, as shown in table 2, and redispersed.

**Table 2:** A summary of the different AuNP solutions used throughout the experiments.

| Amount of concentrated AuNP pellet | Composition of solution | Use |
|---|---|---|
| 20 µl/ml solution | $10^{-2}$ M citrate buffer | All nanoparticle deposition experiments |
| 6.66 µl/ml solution | MilliQ water | UV-Vis, determining concentration of AuNP solutions |
| 20 µl/ml solution | MilliQ water | Zeta potential measurement |
| 20 µl/ml solution | $10^{-2}$ M citrate buffer | Zeta potential measurement |
| 20 µl/ml solution | $10^{-4}$ M citrate buffer | Zeta potential measurement |
| 20 µl/ml solution | $10^{-6}$ M citrate buffer | Zeta potential measurement |
| 20 µl/ml solution | $10^{-8}$ M citrate buffer | Zeta potential measurement |

## 3.2 UNIFORM NANOPARTICLE DEPOSITION ON GLASS SUBSTRATES

Uniform deposition was performed on two glass cover slides. The protocol that was used corresponds to the densest region of Cline Scientific's AuNP gradients on glass, meaning that the two samples can be used as benchmarks; the number density of AuNPs on polystyrene substrates should be of comparable size for the respective functionalisation method to be of use for the gradient application.

First, the substrates and glassware (10 ml beakers) were cleaned with a solution similar to "base piranha", consisting of a 5:1:1 mixture of MilliQ water, hydrogen peroxide ($H_2O_2$) and ammonium hydroxide ($NH_4OH$). The solution was heated to 85 °C and allowed to react for 10 minutes, after which substrates and glassware were rinsed thoroughly with MilliQ water.

Before the silanisation, surfaces and glassware were rinsed thoroughly with methanol. The substrates were silanised for 1 hour in room temperature (covered by aluminium foil) using an APDMES solution (3-aminopropyldimethylethoxysilane, 97 %, prod. nr. AB110423, abcr) diluted 10 times with methanol. After the silanisation, the surfaces were again rinsed thoroughly with methanol.

Before conducting the AuNP deposition, the surfaces were rinsed with MilliQ water. The nanoparticle depositions were performed by immersing the glass substrates in AuNP solutions (20 µl AuNP pellet/ml 10 mM citrate buffer) for 30 minutes in room temperature (covered by aluminium foil). The deposition was stopped by replacing the AuNP solution with MilliQ water. Directly after deposition (when still in MilliQ water), the glass surfaces were pink. Upon drying, the glass surfaces turned a darker colour, probably due to agglomeration.

## 3.3 EXPERIMENTS ON POLYSTYRENE SUBSTRATES

The experiments on polystyrene substrates consisted of fabrication and functionalisation of substrates.

### 3.3.1 FABRICATING POLYSTYRENE SUBSTRATES

Approximately 0.3 g polystyrene pellets (amorphous, $M_w$ ~192 000, prod. nr. 430102-1KG, Sigma-Aldrich) were used to create each substrate. The pellets were placed in a metal pressing frame, containing two rows of four hollow spaces with rounded corners (inner dimensions 11x15x2 mm). The pressing frame was placed between two PET films, which were placed between two metal plates, creating a sandwich setup.

The sandwich was then placed between the heating plates of the press (position A in figure 10), which were preheated to 180 °C. The pressing procedure consisted of preheating the samples at 180 °C for 3 minutes, raising the pressure to 10 tonnes, keeping the pressure and temperature at 10 tonnes and 180 °C for 3 minutes (the pressure normally had to be adjusted a few times) and finally lowering the pressure, removing the sample from the press and cooling the sample under pressure, using refrigerated weights. The substrates were then removed from the pressing frame and checked for irregularities. Samples showing signs of pellets not having fused properly were disposed of. Before using the substrates in subsequent experiments, they were cleaned by placing one drop of detergent on the surface, rubbing gently and rinsing with plenty of MilliQ water. The surfaces were then blow-dried with nitrogen ($N_2$).

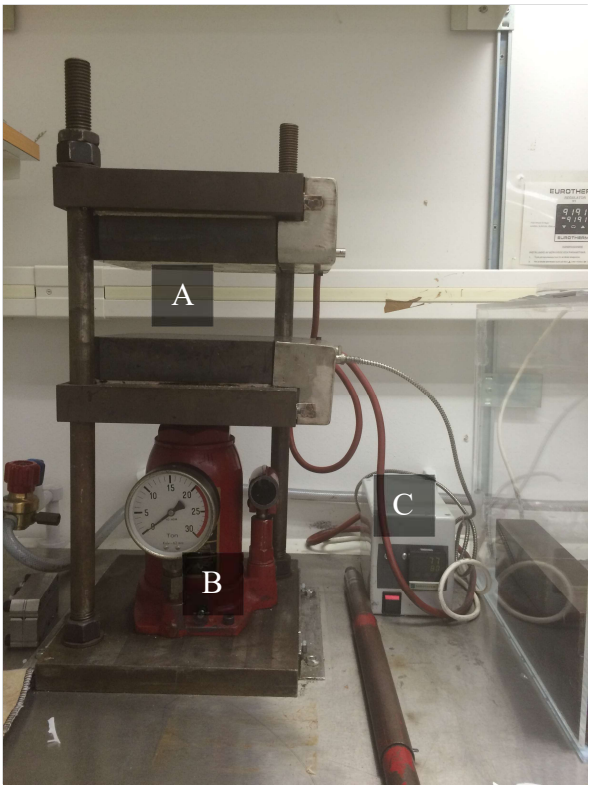


**Figure 10:** The system used for pressing the polystyrene substrates. A: The two heated plates, where the samples were placed. B: Press with manometer. C: Regulator for controlling the temperature of the plates.

### 3.3.2 FUNCTIONALISING THE POLYSTYRENE SUBSTRATES

As described in section 2.2, at least two different paths of rendering polystyrene surfaces positively charged are available [20, 21, 22, 24, 23]. Both paths were tested:

- Silanisation, with $O_2$ plasma, UV/$O_3$ treatment or (base) piranha wash as oxidising pre-treatments
- Coating with positively charged substance (poly-l-lysine), with $O_2$ plasma as pre-treatment for increased surface wettability

All functionalisation procedures were performed as described below. The silanisation was performed as for the glass substrates, described in section 3.2.

**$O_2$ plasma**

Plasma treatment was carried out using a radio frequency plasma generator (Plasma Cleaner, Harrick Plasma) equipped with a gas mixer (Plasmaflo, PDC-FMG, Harrick Plasma), controlling the flow rate of gas and monitoring the pressure in the chamber. The system was connected to a vacuum pump (nXDS Scroll Pump, Edwards).

The sample was placed in the chamber and the vacuum pump was turned on, lowering the pressure to less than 300 mTorr (approximately 40 Pa). The chamber was then refilled with $O_2$ gas. This evacuating/refilling procedure was performed 3 times, ensuring that the chamber contained mostly $O_2$ gas. The $O_2$ gas flow was then set to 10 SCCM (standard cubic centimetres per minute), resulting in an operating pressure stabilising at approximately 1600 mTorr (213.3 Pa). The plasma generator was turned on to high intensity and left running for 30 minutes, after which the pressure typically had dropped to approximately 1550 mTorr

(206.6 Pa). The samples were then either silanised, as described in section 3.2, or coated with poly-l-lysine. A considerable increase of water contact angle was noticed during subsequent experiments.

**UV/$O_3$ treatment**
The ozone treatment was performed using an ozone cleaning system (UVOH 150, FHR Anlagenbau GmbH). The $O_2$ flow was set to 0.5 SCCM and the mercury lamp was turned on for 60 minutes. The samples were then silanised, as described in section 3.2.

**Base piranha wash**
The procedure was performed as when cleaning the glass substrates, described in the second paragraph of section 3.2. The polystyrene substrates had a tendency to float during the procedure, but the samples were turned so that the surface that would be deposited on was facing down into the piranha wash. The samples were then silanised, as described in section 3.2.

**Coating with poly-l-lysine**
The samples were pre-treated with $O_2$ plasma, as previously described, to increase the wetting ability of the poly-l-lysine hydrobromide solution (0.25 mg/ml in water). Early experiments, albeit performed on polystyrene substrates cut from a polystyrene microscope glass and 100 nm AuNPs, indicated that 10 minutes of $O_2$ plasma treatment was enough to get even coverage of AuNPs (thereby also indicating even deposition of poly-l-lysine). The deposition of AuNPs in these experiments was observed in a dark field microscope. For practical reasons, the surface presented in the results underwent 30 minutes of $O_2$ plasma.

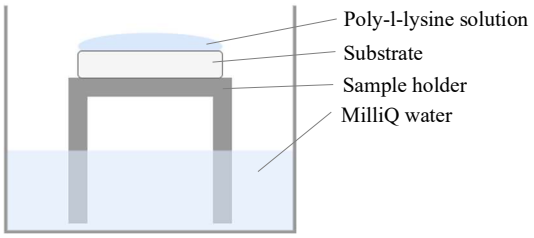


**Figure 11:** Schematic picture, illustrating the experimental set-up for coating substates with poly-l-lysine.

The coating was performed by placing a sample holder, looking somewhat like a table, in a glass Petri dish. The floor of the Petri dish was covered with MilliQ water, so as to prevent the poly-l-lysine from drying out during the experiment. The surface of the sample was then covered with the poly-l-lysine solution, after which the Petri dish was covered and left for 10 minutes. To stop the coating procedure, the sample was immersed in MilliQ water and blow-dried with $N_2$, after which nanoparticle deposition was performed.

### 3.3.3 DEPOSITING GOLD NANOPARTICLES ON POLYSTYRENE SUBSTRATES
The deposition of nanoparticles was performed in the same manner as on glass substrates, described in the last paragraph of section 3.2. A summary of the different samples used in the results is presented below:

- Untreated polystyrene
- Silanised polystyrene, without pre-treatment
- Silanised polystyrene, pre-treated with base piranha wash
- Polystyrene coated with poly-l-lysine, pre-treated with $O_2$ plasma (30 minutes)

- Silanised polystyrene, pre-treated with $O_2$ plasma (30 minutes)
- Silanised polystyrene, pre-treated with UV/$O_3$ (60 minutes)

In all deposition experiments but one (the untreated polystyrene), the glassware was cleaned via the base piranha wash as described in section 3.2. Due to time limitations, the glass beaker used in the experiment with untreated polystyrene was only rinsed with plenty of MilliQ water.

Upon AuNP deposition, the samples normally showed some blue/pink colour. The colour was, by far, most intense for the silanised polystyrene that was pre-treated with UV/$O_3$, though seemingly fainter than the colour of the glass samples. The polystyrene coated with poly-l-lysine also showed distinct blue/pink colour. The other samples showed very little, if any, colour.

## 3.4 CHARACTERISING THE SYSTEM

Nanoparticle solutions were characterised using UV-Vis spectroscopy and zeta potential measurements and the surfaces were mainly characterised using SEM and analysing the pictures with Ripley's K and L functions.

### 3.4.1 UV-VIS SPECTROSCOPY

UV-Vis spectroscopy was performed using an Evolution 60 UV-Vis spectrophotometer (Thermo Scientific). The baseline was measured with MilliQ water and the scanning speed was set to "medium", scanning from 400 to 700 nm in steps of 1 nm.

Nanoparticle batch solutions were characterised to ensure that AuNPs were of correct size. The sample for determining AuNP concentration was prepared as described in table 1. As described in the table, the sample for determining AuNP concentration was diluted by a dilution factor of 3, which was needed in order to lower the absorption (without dilution, the absorption reached values higher than 3.5, resulting in large deviations in the measured spectrum).

The size and concentration of AuNPs were calculated using eq. (1) and (2), respectively. The previously mentioned dilution of the solution for determining AuNP concentration was compensated for by multiplying the calculated AuNP concentration with the dilution factor, assuming linear behaviour from the Lambert-Beer law.

### 3.4.2 ZETA POTENTIAL

Zeta potential measurements were executed using a Zetasizer Nano ZS ZEN3500 (Malvern Instruments), fitted with a 532 nm laser.

Before conducting measurements, the laser was turned on for at least 30 minutes, allowing for the laser to stabilise. The sample solutions, described in table 1, were then injected in a disposable folded capillary cell (DTS1060) and 3 sets of measurements, each set containing 100 measurements, were performed on each sample. Due to a lack of capillary cells, the same disposable cell was used in all measurements. After each measurement, the cell was cleaned by rinsing it with plenty of distilled water. The samples were analysed in increasing order of citrate buffer to prevent solutions of high ionic strength contaminating samples of low ionic strength.

Parameters for the samples were chosen from a database in the software. The database had an entry for AuNPs, but not for citrate solution, to the solution was approximated as water.

Consequently, the samples were given parameters as presented in table 3 in the subsequent analysis.

**Table 3:** Parameters used in the zeta potential measurements. The parameters were kept constant for all samples.

| AuNPs | | Dispersant (water) | | | |
|---|---|---|---|---|---|
| **Refractive index (-)** | **Absorption (-)** | **Temperature (°C)** | **Viscosity (cP)** | **Refractive index (-)** | **Dielectric constant (-)** |
| 3.090 | 0.345 | 25.0 | 0.8872 | 1.330 | 78.5 |

During the experiments, most experiments showed decreasing trend of measured zeta potential, implying that the results are somewhat imprecise. The cause may be that the AuNP solution is too concentrated, as for the UV-Vis spectroscopy, or that the set-up is not suitable for the samples (the instruction manual mentions that laser in the current system is least suitable for red samples).

### 3.4.3 Scanning Electron Microscopy (SEM)

All pictures were taken using a SUPRA 60VP SEM (Carl Zeiss AG). Due to polystyrene and glass being electrical insulators, all samples were spin coated (at 4000 RPM for 45 seconds) with the conducting polymer Espacer 300Z before the analysis. The acceleration voltage was normally set to 10-12 kV. The setting for each picture is indicated in the results. Pictures were taken at different magnifications, often ranging from 100 000 to 600 000 times magnification, and representative pictures were chosen for subsequent analyses.

### 3.4.4 Spatial descriptive statistics

Images were loaded into MATLAB and particle coordinates were manually collected using the command ginput. The coordinates were then converted from pixels to nm, expressed as the distance from the top left corner of the picture, by using a conversion factor obtained by measuring the scale bar of the SEM pictures in ImageJ.

Ripley's K and L functions were evaluated for the collected coordinates using the spatstat package in R. By using the command envelope, 99 simulations of complete spatial randomness were performed, creating an empirical band (envelope) for the subsequent analysis – if the observed estimation of the L function was below (or above) the envelope, the sample was considered showing statistically significant dispersion (or clustering). The functions were also used to evaluate the results from the computational model, presented in the following section.

## 3.5 Modelling nanoparticle adsorption

The purpose of the rudimental computational model was to increase the understanding of the AuNP deposition process by employing the theory as outlined in section 2.3. The model was designed as a Monte Carlo simulation and the general principle of the model was to estimate the AuNP adsorption at different maximum particle-substrate potentials, $W_{ps,max}$, thereby estimating AuNP number density as a function of $W_{ps,max}$. Furthermore, the computed AuNP coordinates at some $W_{ps,max}$ were analysed in terms of Ripley's L function to give insight on the computed AuNP dispersion behaviour.

The model was constructed in MATLAB, using the theory of nanoparticle adsorption as outlined in section 2.3. Figure 9 outlines the computational steps that were employed for 100

different values of $W_{ps,max}$, ranging from 0 to 5 $k_bT$ J (at $T = 294.15$ K). As shown in figure 12, the steps include: first, calculating the number of AuNPs diffusing to the vicinity of the substrate surface – the AuNPs that are available for adsorption to the substrate – then, performing stochastic tests to determine if the AuNPs adsorbs to the substrate.

There is one stochastic test for the substrate-particle interaction, governed by eq. (10) at current $W_{ps,max}$, and one stochastic test for the particle-particle interactions to the AuNPs already adsorbed to the substrate surface, governed by eq. (3), (5) and (11). The stochastic tests are performed by assigning a random value, $p$, to the AuNP, assuming uniform distribution ($p \sim U(0,1)$). Then $p$ is compared to $P_2$ – the probability of adsorbing to the substrate, as per eq. (10) and (11). If $p \in [0, P_2]$ in both tests (separate $p$ is assigned at each test and different $P_2$ in each test), the AuNP adsorbs to the substrate surface.

To be able to estimate the average AuNP number density at current $W_{ps,max}$ and providing an empirical confidence interval for the AuNP number density, the steps in figure 12 were repeated 100 times for each value of $W_{ps,max}$. That is, the steps in figure 12 were employed 100x100 times for each value of $W_{ps,max}$ in total.

It should be noted that the model contains several approximations due to lack of material data and to facilitate the model, mainly:

- The dielectric constant of the solvent (citrate solution) is assumed to be similar to that of water.
- The surface potential of the AuNPs is approximated as the measured zeta potential.
- The dynamic viscosity of the citrate solution is assumed to be similar to that of water.
- The citrate solution is assumed to dissociate completely, so that ion concentration can be easily calculated from bulk concentration of the salt.

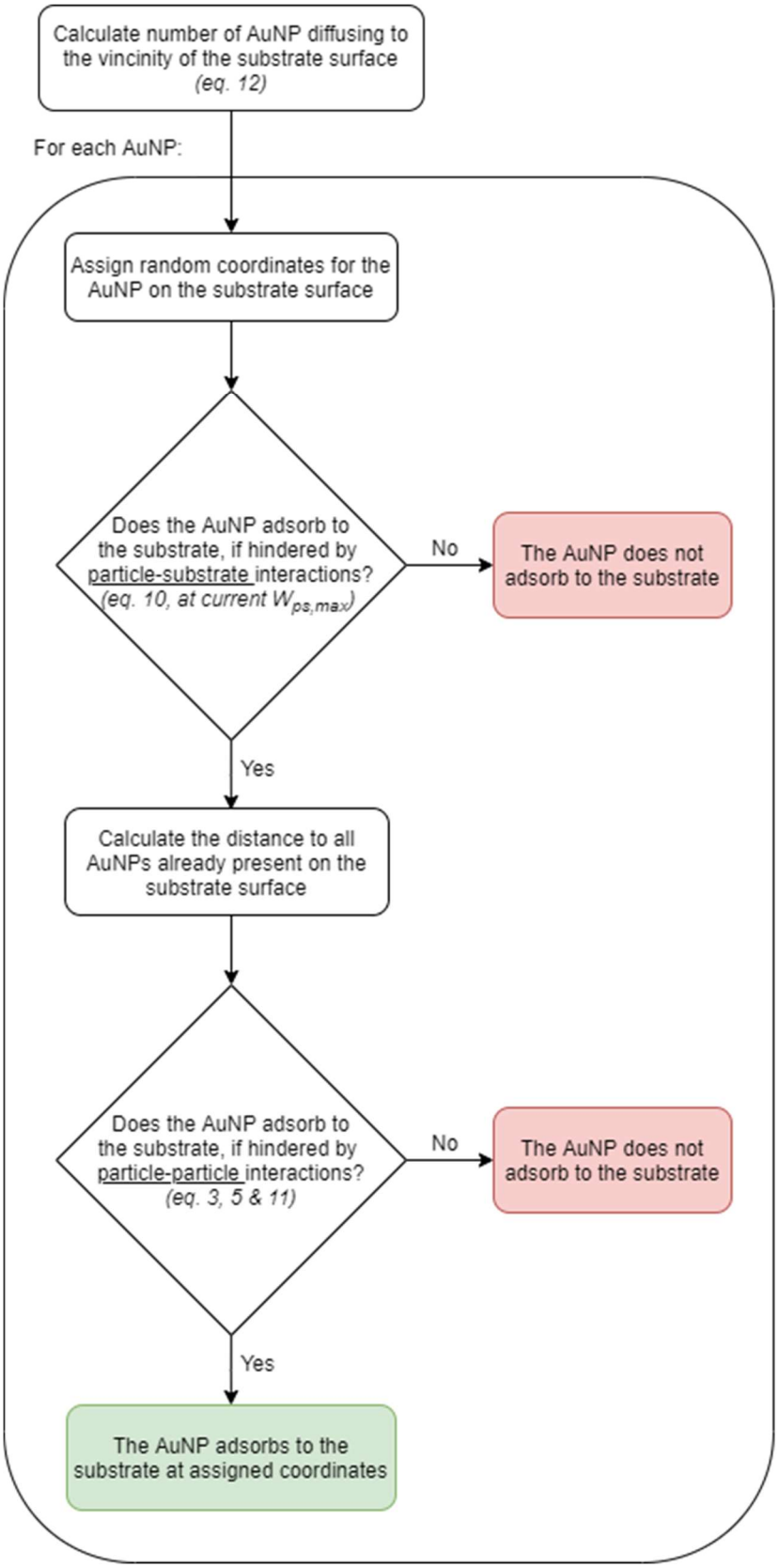


**Figure 12:** Schematic model of the computational model for AuNP adsorption.

# 4 RESULTS AND DISCUSSION

The experimental results evaluated in this chapter comprise nanoparticle characterisation and uniform nanoparticle adsorption on glass and polystyrene substrates, and the implications for nanoparticle gradient application on polystyrene is evaluated. Additionally, the computational model for AuNP adsorption is evaluated.

## 4.1 NANOPARTICLE CHARACTERISATION

Different nanoparticle solutions used in the experiments, as listed in table 2, were characterised with UV-Vis spectroscopy and zeta potential measurements.

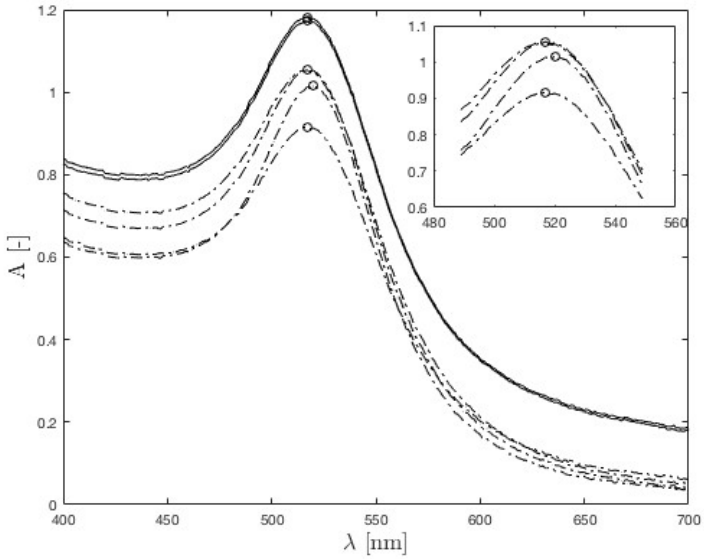


**Figure 13:** UV-Vis spectra for AuNP solutions. The four dashed lines correspond to four different fresh AuNP solutions (batch) and the two solid lines are two samples from the same concentrated AuNP solution. The circles indicate $\boldsymbol{\lambda_{SPR}}$.

Starting with the batch solutions, shown as dashed lines in figure 13, it is noted that all four solutions exhibit similar UV-Vis spectra. As seen in the indent, three out of four solutions show approximately the same $\lambda_{SPR}$ (517 nm). The fourth solution shows a slightly larger value (520 nm), indicating a slightly larger particle size by eq. (1). Other solutions prepared using the same protocol show the same behaviour, indicating that the protocol results in similar particles, though some exceptions can occur, probably caused by variations in temperature.

For the concentrated AuNP solutions (prepared by centrifuging batch solution and redispersing in MilliQ water), shown as solid lines in figure 13, is noted that the $\lambda_{SPR}$ is the same as for the majority of the batch solutions (517 nm), again indicating similar AuNP size. Since the concentrated solutions use water as dispersant, eq. (1) and (2) is employed to determine the size and concentration of the AuNPs.

**Table 4:** Calculated AuNP size and concentration for the two concentrated samples. Size and concentration were calculated using both the experimental and theoretical parameters from [13].

| $A_{SPR}$ | $A_{450}$ | Size (nm) | | Concentration ($m^{-3}$) | |
|---|---|---|---|---|---|
| | | Experimental | Theoretical | Experimental | Theoretical |
| 1.18 | 0.81 | 9.04 | 8.15 | $1.08 \cdot 10^{19}$ | $1.49 \cdot 10^{19}$ |
| 1.17 | 0.79 | 9.31 | 8.44 | $0.98 \cdot 10^{19}$ | $1.32 \cdot 10^{19}$ |

As shown in table 4, the absorption values for the two concentrated samples vary by approximately 1-2 %, resulting in deviations in size and concentration of approximately 3-3.5 % and 10-13 %, respectively. This enhanced effect is probably a result of the exponential behaviour of the functions, as seen in eq. (1) and (2).

As noted in section 2.1.1, using experimental parameters results in an improved deviation [13]. Consequently, nanoparticle size and concentration are determined using the average of experimental values in table 4, resulting in an estimated size of 9.17 nm and a concentration of approximately $3.09 \cdot 10^{19}$ $m^{-3}$ (after correcting with the dilution factor).

Concentrated samples with varying citrate buffer concentration and a sample of fresh batch solution were characterised using zeta potential measurement. The results provided knowledge on the stability of the particle solution and were used in the computational model.

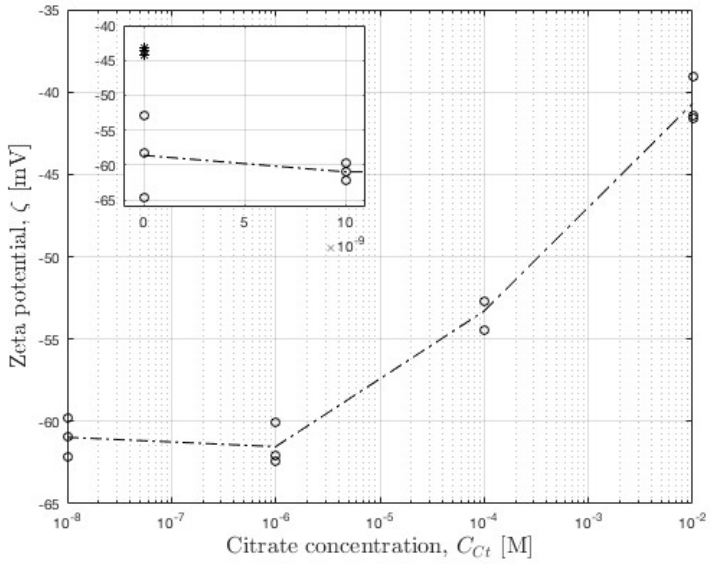


**Figure 14:** Zeta potential measurements for AuNPs in solutions of varying citrate buffer concentrations. The insert shows the graph extended to 0 M (MilliQ water). The values represented with circles were used in subsequent analysis, whereas values marked with asterisks were excluded (see discussion below). The dashed line runs through the average zeta potential for each citrate concentration. Note the logarithmic x-axis of the main plot.

Figure 14 shows the zeta potential for concentrated AuNP solutions of varying citrate buffer concentration. The figure indicates a positive trend for concentrations higher than $10^{-6}$ M, whereas the potential seems to be quite stable at around -60 mV for concentrations below $10^{-6}$ M. The samples of higher zeta potential in the indent was excluded, as they were assumed to be false measurements. This assumption was done, since those samples were measured directly after a solution of higher ionic strength. The higher zeta potential could thus arise from leftover sample volume of higher ionic strength, lowering the potential as per eq. (5). Overall, the behaviour is expected, as increasing ionic strength should decrease the potential, but when comparing the zeta potential value in MilliQ with those stated in section 2.1.2, the measured values seem rather low. As noted, this might be an effect of the high concentration of AuNPs, making measurements imprecise, or the laser not being optimal for the sample, as noted in section 3.4.2.

## 4.2 UNIFORM NANOPARTICLE DEPOSITION ON GLASS SUBSTRATES

Two glass substrates with nanoparticle density corresponding to the densest region of Cline Scientific's AuNP gradient product were fabricated using standard procedure. Using data from figure 10 B and D, shown below, the AuNP densities of the samples were estimated to $2.12 \cdot 10^{15}$ $m^{-2}$ and $2.84 \cdot 10^{15}$ $m^{-2}$, respectively, resulting in an average AuNP density of $2.48 \cdot 10^{15}$ $m^{-2}$. This result is then used as a benchmark for the other samples; the AuNP density should be of similar order to be of use in a AuNP number density gradient application.

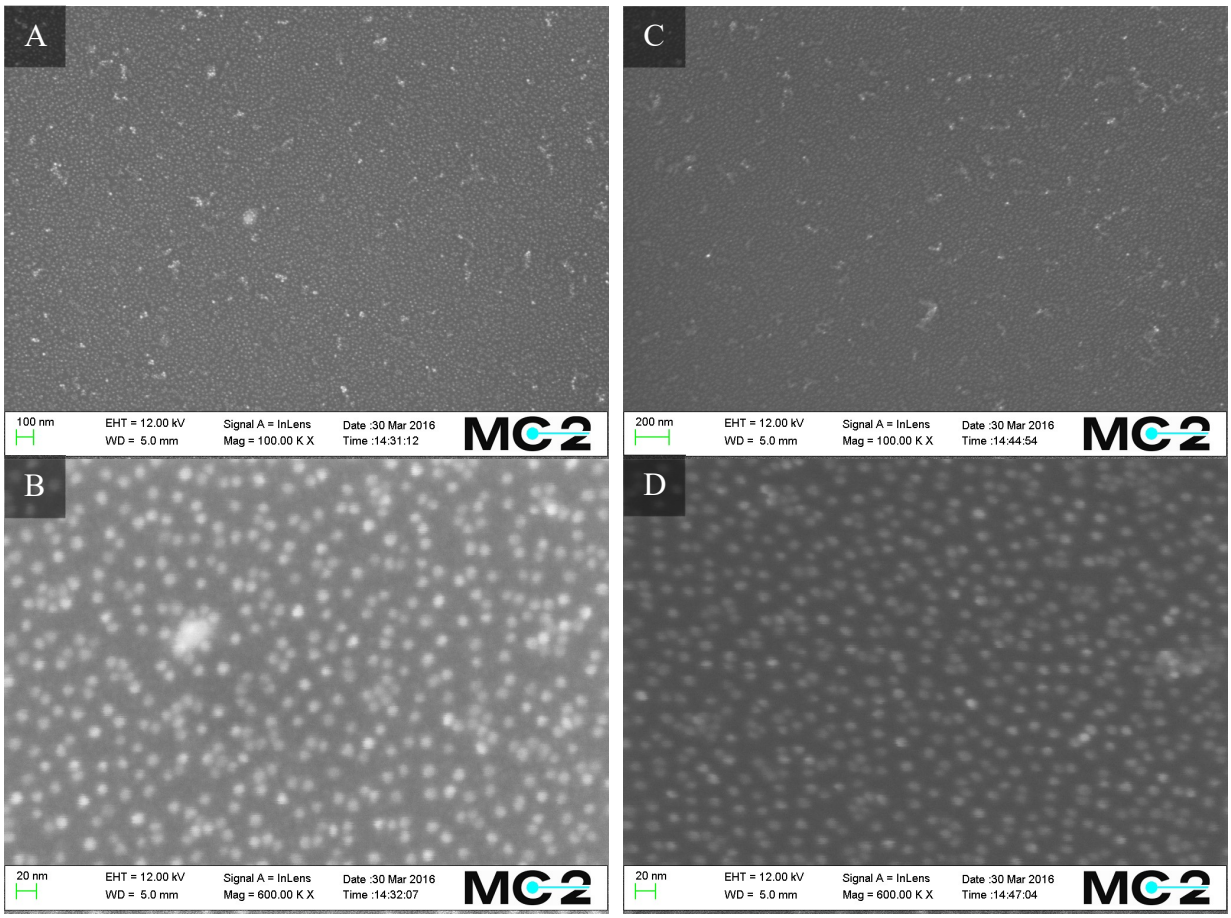


**Figure 15:** Nanoparticle deposition on two glass substrates. The two columns (pictures A-B and C-D) show one sample each. A and C: At 100 000 times magnification, both samples show dense AuNP deposition and some agglomeration. B and D: At 600 000 times magnification, individual AuNPs are clearly visible on both samples.

As seen in figure 15 A and C, the samples display some AuNP agglomeration. This probably occurred during drying, as noted in section 3.2, which might be explained by water droplets "dragging" nanoparticles around when rolling over the surface during the drying procedure.

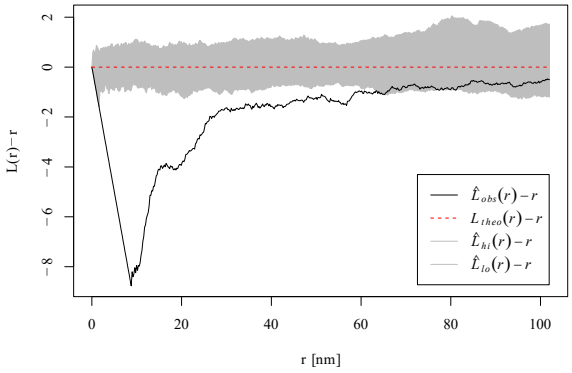


**Figure 16:** Ripley's L function evaluated for the glass substrate shown in the left column of figure 15, using coordinates from figure 15 B.

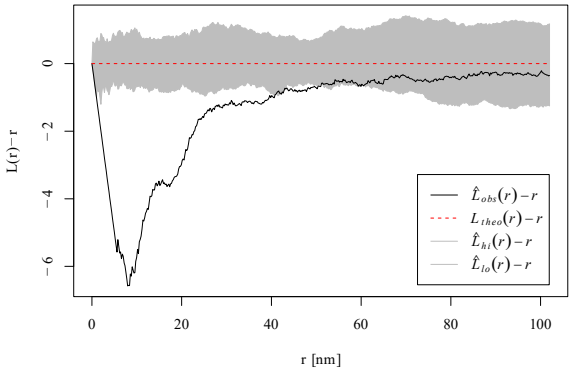


**Figure 17:** Ripley's L function evaluated for the glass substrate shown in the right column of figure 15, using coordinates from figure 15 D.

The surfaces were further characterised by analysing the coordinates of the AuNPs in figure 15 B and D using Ripley's K and L functions. The result for the L function, presented in figures 16 and 17, indicate significant dispersion occurring for interparticle distances up to 40-60 nm. The behaviour up to 10 nm has an obvious explanation; since the interparticle distance, $r$, is defined as the distance between particle centres, no particles should be closer than approximately $2R$ ($\approx$ 9.17 nm, using the mean of the experimental values from section 4.1). The separation for larger interparticle distances probably stems from repulsive electrical double layer interactions, as explained in section 2.3.1 and 2.3.3. Thus, it seems as though the glass substrates exhibit the crucial property of interparticle interactions limiting the adsorption, so that the interparticle distance can be controlled by varying the ionic strength. It is also noted that the deposition pattern goes back to complete random ($L(r) - r \approx 0$) for larger interparticle distances, indicating that the force diminished after some distance.

## 4.3 UNIFORM NANOPARTICLE DEPOSITION ON POLYSTYRENE SUBSTRATES

In the following sections, the AuNP deposition results on polystyrene substrate with different functionalisation methods are presented.

### 4.3.1 UNTREATED POLYSTYRENE

As previously mentioned, the untreated polystyrene was meant to be used as a reference sample, determining how much AuNPs attaches without any additional surface treatment.

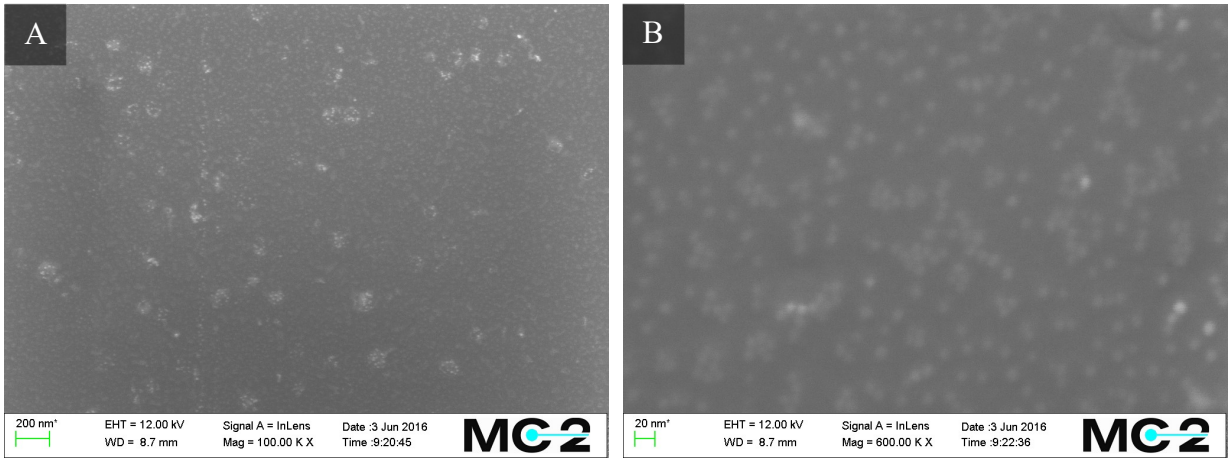


**Figure 18:** SEM pictures of AuNPs deposited on an untreated PS substrate. A: At 100 000 times magnification, several circular areas of unknown nature are visible. B: At 600 000 times magnification, individual AuNPs are clearly visible.

Unexpectedly, figure 18 shows dense AuNP attachment. In figure 18 B, the nanoparticle density was estimated to approximately $1.68 \cdot 10^{15}$ $m^{-2}$, which is similar to the density on the reference glass sample, indicating that no treatment at all could be of interest for the final product. However, as the theory suggests that only little – if any – AuNPs should attach, due to untreated polystyrene having no inherent charge or any attracting functional groups, one could suspect that something went wrong in the deposition process, probably caused by contaminants.

Dirt is a plausible contaminant, supported by the fact that that the glassware used in the experiment was not cleaned using the standard procedure. Another plausible cause of contamination is leftover detergent from the cleaning procedure. Both of these contaminants would affect the hydrophobic interactions. Leftover detergent could decrease the surface energy between AuNPs and polystyrene, thereby facilitating the deposition. Dirt could cause a boundary layer between a polar and nonpolar phase, which the AuNPs seemingly are attracted to.

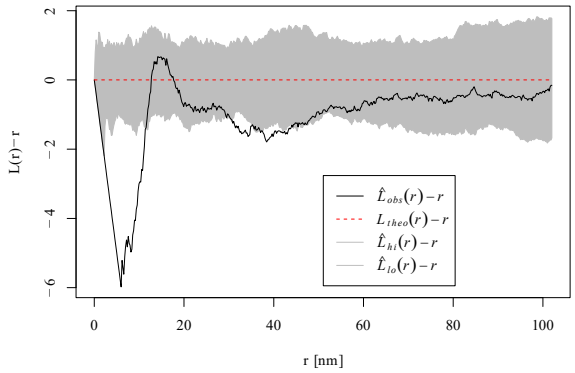


**Figure 19:** Ripley's L function evaluated for the untreated polystyrene substrate, using coordinates from figure 18 B.

To further characterise the nanoparticle deposition, the coordinates of the AuNPs in figure 18 B were analysed using Ripley's K and L functions. The results in figure 19 indicate significant dispersion occurring only for distances below approximately 10 nm. Since the interparticle repulsion does not seem to be limiting the deposition, the alternative of depositing AuNPs directly on untreated is not considered as a promising alternative. This holds true regardless of whether the high AuNP density is an experimental error or not; either the high AuNP density is correct, but the deposition cannot be controlled by changing the ionic strength of the solution or the AuNP density is false and the real density is much lower, resulting in a too sparse gradient for AuNP number density gradient application at Cline Scientific.

### 4.3.2 SILANISED POLYSTYRENE, WITHOUT PRE-TREATMENT

AuNP deposition on clean polystyrene treated with APDMES was conducted to determine whether silanisation and subsequent AuNP adsorption could be performed without pre-treating the polystyrene surface.

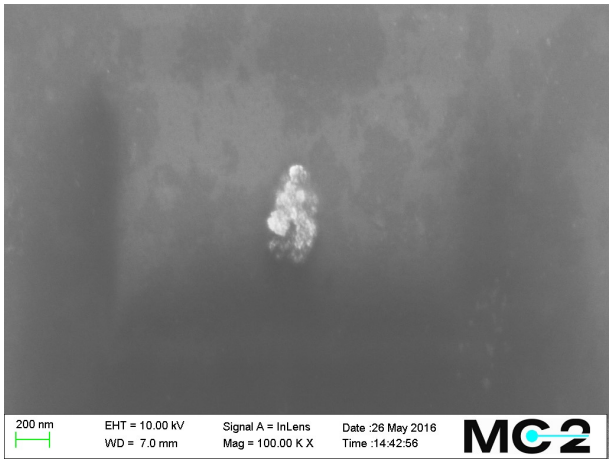


**Figure 20:** SEM picture of AuNP deposition on polystyrene treated only with APDMES. The pictures showed some dust particles on the sample, but no AuNPs.

As expected, figure 20 shows no AuNPs depositing on the surface. This effect probably stems from no APDMES having silanised the surface, in accordance with the theory presented in section 2.2. Another contributing factor for the lack of deposition could the hydrophobic nature of untreated polystyrene; since the citrate stabilised AuNPs are negatively charged, they should exhibit more affinity for polar substrates. As no AuNP attachment was detected, the sample was not analysed further.

### 4.3.3 SILANISED POLYSTYRENE, PRE-TREATED WITH BASE PIRANHA WASH

Due to the oxidative nature of the base piranha wash, described in section 2.2, the hypothesis was that the process might be able to oxidise the surface of polystyrene to some degree, maybe introducing the hydroxyl groups necessary for successful silanisation with APDES.

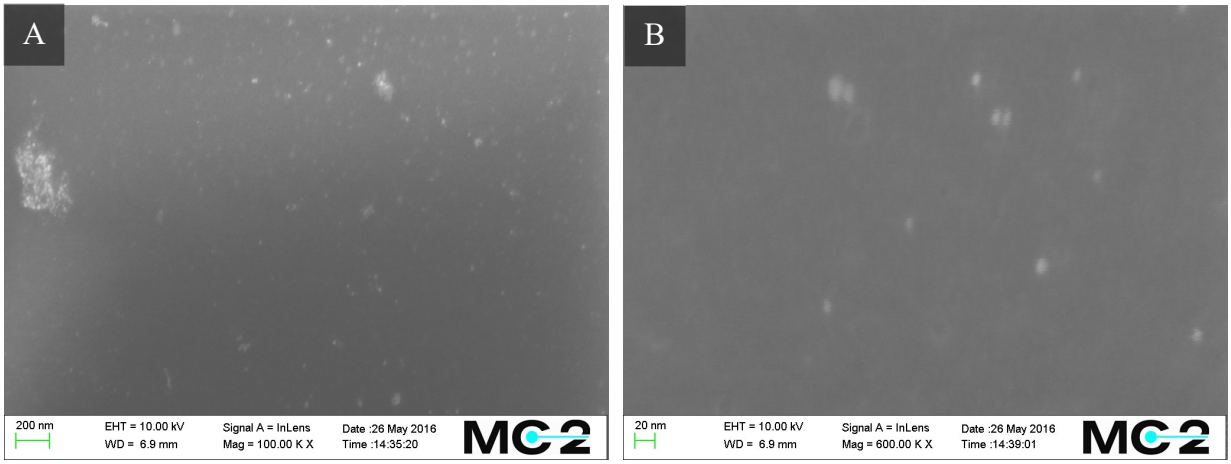


**Figure 21:** SEM picture of AuNP deposition on polystyrene treated with APDMES, after pre-treatment with base piranha wash. A: At 100 000 times magnification, some dirt and AuNPs are visible (both agglomerated and dispersed). B: At 600 000 times magnification, individual AuNPs are clearly visible.

The SEM pictures seen in figure 21 show a rather sparse AuNP deposition, indicating that if oxidation occurred, only few hydroxyl groups were formed. Using figure 21, the nanoparticle density was estimated to $5.30 \cdot 10^{13}$ $m^{-2}$, which is significantly lower than the density on the glass surfaces. Consequently, the method should be of no use in a final product. Even so, the coordinates were analysed using the Ripley's K and L functions.

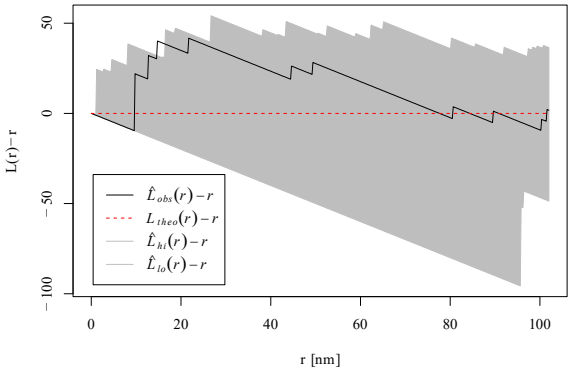


**Figure 22:** Ripley's L function evaluated for silanised polystyrene, pre-treated with base piranha wash, using coordinates from figure 21 B. Note the wide envelope, caused by the low number of AuNPs.

Figure 22 shows a broad envelope, implying that conclusions on dispersion and clustering should not be drawn. This behaviour is expected, since the number of coordinates in the analysis looks too low to determine the adsorption pattern properly. The base piranha wash was probably not oxidative enough. As previously described, normal piranha wash might have been better, but could have damaged the surface too much.

### 4.3.4 POLYSTYRENE COATED WITH POLY-L-LYSINE, PRE-TREATED WITH $O_2$ PLASMA

Poly-l-lysine was expected to result in a dense nanoparticle deposition, since it's a general method of introducing positive charge on a substrate [23].

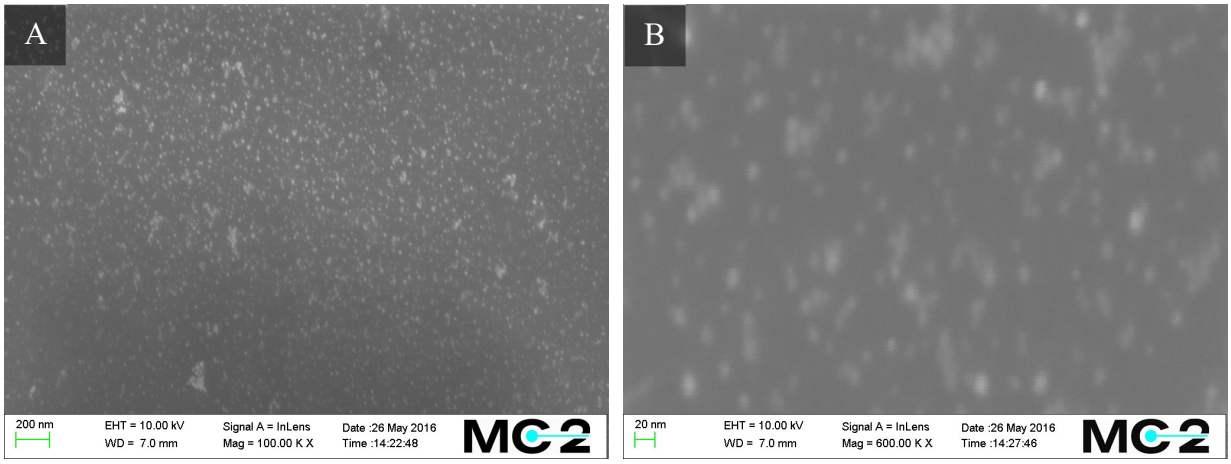


**Figure 23:** SEM pictures of polystyrene coated with poly-l-lysine and pre-treated with $O_2$ plasma. A: At 100 000 times magnification, dense AuNP deposition and some agglomeration is shown. B: At 600 000 times magnification, individual AuNPs are easily distinguishable.

From figure 23 B, the nanoparticle density is estimated to $9.39 \cdot 10^{14}$ $m^{-2}$, which is similar to the density on glass ($2.48 \cdot 10^{15}$ $m^{-2}$). The high AuNP density would imply that it is a suitable method.

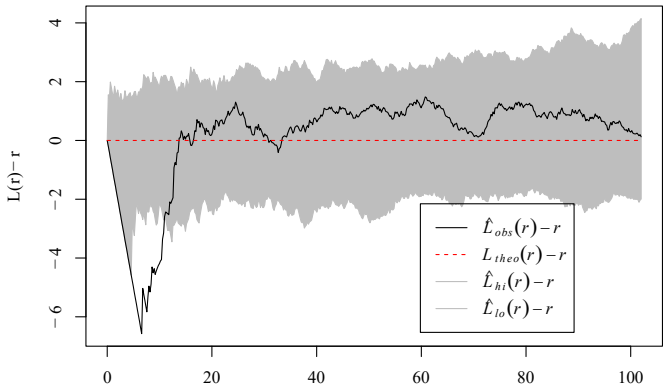


**Figure 24:** Ripley's L function evaluated for polystyrene coated with PLL and pre-treated with $O_2$ plasma. Coordinates are taken from figure 23 B.

However, figure 24 shows interparticle repulsion only at the distance where it has to occur following the particle size (*2R*), so the method does not show the correct behaviour necessary for creating the AuNP gradient. The exact reason is unclear, but there might be ions (HBr) present close to the poly-L-lysine, thereby reducing the interparticle repulsion. Also, the polymer itself might affect the deposition in some way.

### 4.3.5 SILANISED POLYSTYRENE, PRE-TREATED WITH $O_2$ PLASMA

As noted in section 2.2, this treatment was expected to result mostly in aldehyde/carboxylate species, probably leading to APDMES not being able to silanise the surface.

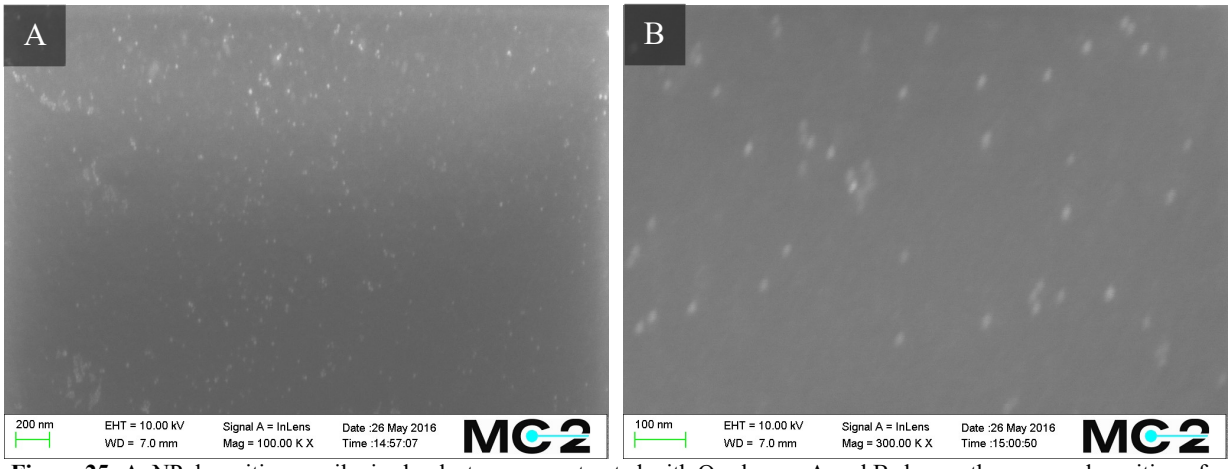


**Figure 25:** AuNP deposition on silanised polystyrene, pre-treated with $O_2$ plasma. A and B show rather sparse deposition of AuNPs.

As shown in figure 25, this treatment exhibits rather sparse deposition of AuNPs, resulting in an AuNP density of $6.16 \cdot 10^{13}$ $m^{-2}$, which is too low to be of use in a final AuNP number density gradient product. As noted, this probably stems from too little APDMES having silanised the surface and, consequently, the surface is probably mainly a polystyrene surface, which has been cleaned and rendered hydrophilic by introducing polar functional groups.

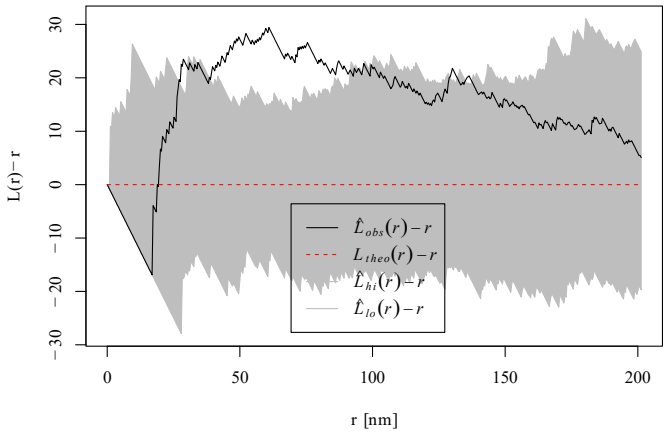


**Figure 26:** Ripley's L function evaluated for silanised polystyrene, pre-treated with O2 plasma. Coordinates are taken from figure 25 B.

In figure 26, clustering is observed for interparticle distances between approximately 30-80 nm. This is an unexpected behaviour, as it would imply that there is an attracting force determining the interparticle distance.

### 4.3.6 SILANISED POLYSTYRENE, PRE-TREATED WITH UV/$O_3$

For the functionalisation path involving silanisation, pre-treatment with UV/$O_3$ was expected to result in the highest AuNP density, because of its documented ability to form less oxidised species on polystyrene, possibly introducing phenol groups [21].

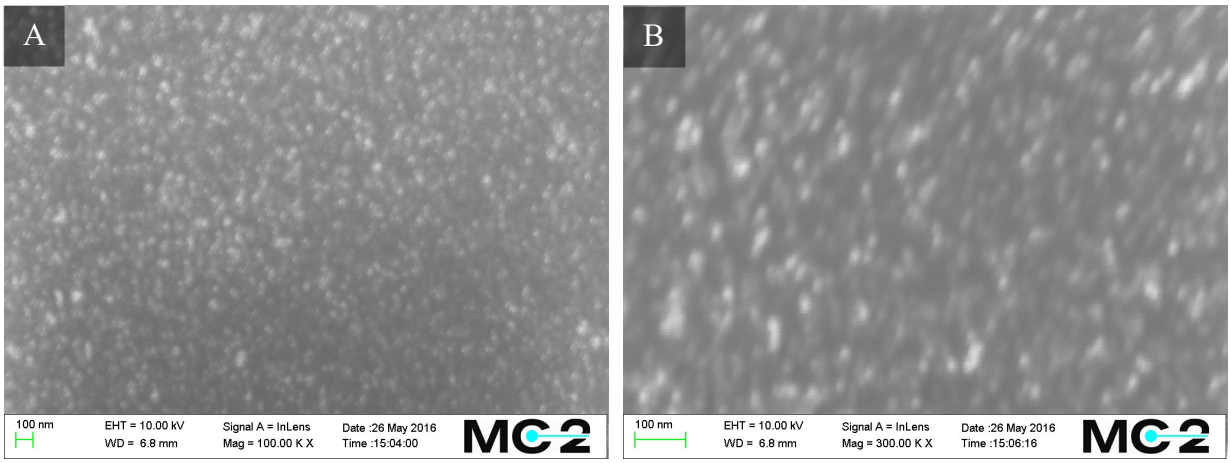


**Figure 27:** Silanised polystyrene, pre-treated with UV/$O_3$. A: the treatment seems to have resulted in a dense and even deposition of AuNPs. B: Dense deposition is observed, though it is hard to distinguish individual particles.

As seen in figure 27, there seems to be dense AuNP deposition, but individual AuNPs are hard to distinguish. Using figure 27 B, the AuNP density was estimated to $5.73 \cdot 10^{14}$ $m^{-2}$, which is of similar order to that on glass. Again, it is plausible that hydroxyl groups were formed on this surface [21], so probably the reason for the high AuNP number density is that the surface was silanised to a high extent.

If comparing to the results in the previous section (4.3.5), UV/$O_3$ treatment showed lower wettability (higher contact angle) than the $O_2$ treatment, but higher AuNP number density. This would indicate that introducing charges on the surface, by silanisation, is more important than rendering the surface more polar/hydrophilic. Consequently, the purpose of the UV/$O_3$

treatment is more to introduce hydroxyl groups for the silanisation than making the surface more hydrophilic.

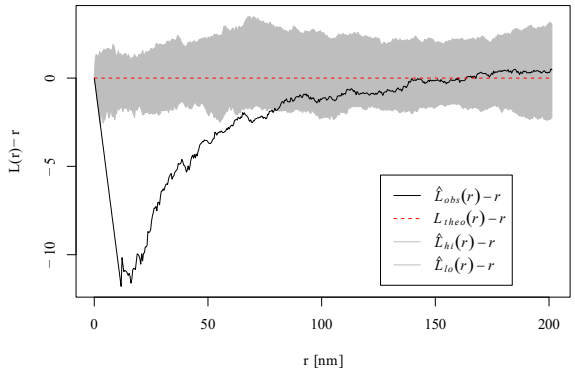


**Figure 28:** Ripley's L function evaluated for silanised polystyrene, pre-treated with $UV/O_3$. Coordinates are taken from figure 27 B.

Furthermore, from figure 28 it is noted that the sample shows a dispersion behaviour for interparticle distances up to approximately 75 nm, which is promising for the use in a number density gradient product.

## 4.4 IMPLICATIONS FOR NANOPARTICLE GRADIENTS ON POLYSTYRENE SUBSTRATES

To be a good candidate for a AuNP number density gradient application on polystyrene, the functionalisation method should two key results:

1. The AuNP number density should be similar as on the glass reference sample.
2. Repulsive interparticle interactions should determine where the AuNPs adsorb to the polystyrene surface, so that the interparticle distance can be tuned by the ionic strength to form a gradient.

According to table 5 below, silanisation with $UV/O_3$ pre-treatment seems like the best alternative, as the AuNP density is similar as on the glass reference samples (same order of magnitude) and the range of dispersion is high.

**Table 5:** Summary of results for the different functionalisation methods. The range of dispersion refers to the interparticle distance at which significant dispersion (as a result of interparticle repulsion) is observed.

| Treatment | AuNP density ($m^{-2}$) | Range of dispersion (nm) | Conclusion |
|---|---|---|---|
| Glass sample, reference | $2.48 \cdot 10^{15}$ | 40-60 | - |
| No treatment | $1.68 \cdot 10^{15}$ | 10 | High AuNP density is probably an experimental error, probably not appropriate for AuNP gradient. |
| Silanisation, no pre-treatment | 0 | - | No AuNP adsorption, not appropriate for AuNP gradient. |
| Silanisation, base piranha wash | $5.30 \cdot 10^{13}$ | 0 | Low AuNP density and no AuNP dispersion observed, not appropriate for AuNP gradient. |
| Poly-l-lysine, $O_2$ plasma | $9.39 \cdot 10^{14}$ | 10 | High AuNP density, but low AuNP dispersion. Probably not appropriate for AuNP gradient. |
| Silanisation, $O_2$ plasma | $6.16 \cdot 10^{13}$ | 0 | Low AuNP density and no AuNP dispersion observed, not appropriate for AuNP gradient. |
| Silanisation, UV/$O_3$ | $5.73 \cdot 10^{14}$ | 75 | High AuNP density and high AuNP dispersion. Might be appropriate for AuNP gradient |

## 4.5 COMPUTATIONAL MODEL OF NANOPARTICLE ADSORPTION

The computational model was used to see if the adsorption behaviour follows the theoretical approach presented in sections 2.3 and to get an estimation of how the maximum barrier height for adsorption affects the nanoparticle density on the samples.

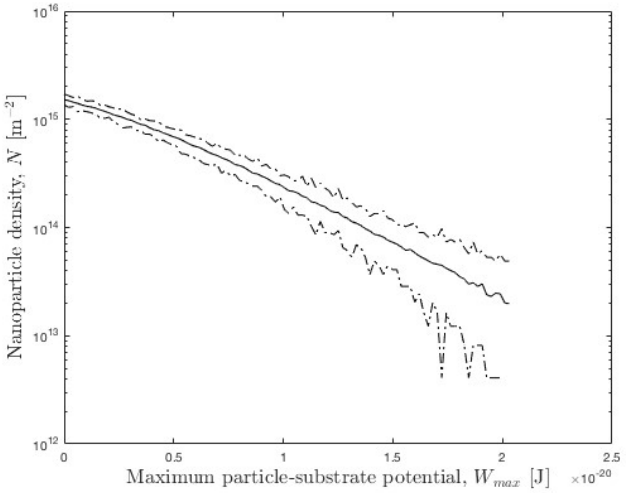


**Figure 29:** Nanoparticle density as estimated by the computational model described in section 3.5. For each value of $W_{max}$, 100 Monte Carlo simulations are made. The solid line represents the average of the 100 simulations for each $W_{max}$, and the dashed lines show the maximum and minimum values.

As described, figure 29 is the result of 100 Monte Carlo simulations for each value of $W_{max}$. As expected from eq. (10) and (11), it shows an exponential dependence for nanoparticle density on the maximum particle-substrate potential and, as such, small changes in in the

potential result in large deviations of the nanoparticle density. Furthermore, it is noted that densities of $2.48 \cdot 10^{15}$ $m^{-2}$ (as for the glass substrates) is only reached with no barrier height, indicating only attractive forces between particles and substrates and that the model is likely underestimating the AuNP density.

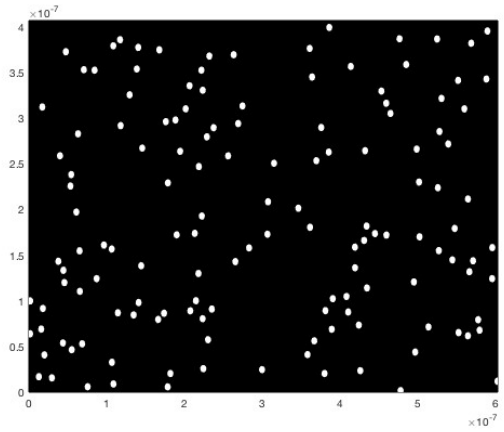


**Figure 30:** One sample picture generated from the computational model. The size of the picture corresponds to a SEM picture at 600 000 times magnification.

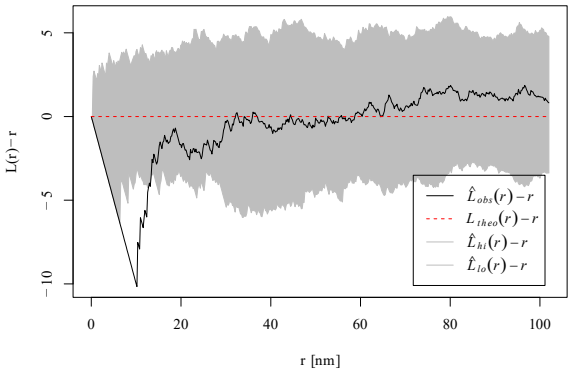


**Figure 31:** Ripley's L function evaluated for the coordinates proposed by the simulation resulting in the deposition shown in figure 30.

Figure 30 shows an example of the AuNP deposition proposed by the computational model for a nanoparticle density of $5.71 \cdot 10^{14}$ $m^{-2}$, which is similar to the one on silanised polystyrene, pre-treated with UV/$O_3$. When analysing the coordinates with Ripley's L function, a similar behaviour is seen as for most of the investigated samples, though with dispersion occurring only at small interparticle distances. Therefore, the result in figure 31 probably indicates that the model underestimates the interparticle repulsion (at least for larger interparticle distances). This could imply that the curve in figure 29 might overestimate the AuNP density, as a higher interparticle potential would result in more particles failing the second test in the computation model (figure 9, eq. 3, 5, & 11).

To summarise, it seems that the model captures the basic phenomena, but underestimates the AuNP density and the interparticle potential (or at least the *range* of the interparticle potential). According to the theory in section 2.3.1, these errors could be explained by several different factors, e.g.:

- Underestimating the number of AuNP diffusing to the vicinity of the polystyrene surface:
  According to eq. (12), underestimating the bulk concentration of AuNPs ($C$) could be a likely cause of error. The concentration is determined from the UV-Vis measurements, e.g. by $A_{450}$ in eq (2), and therefore, UV-Vis measurement error could be a cause of the error. However, as the size of the AuNPs is reasonably estimated by eq (1), which includes $\frac{A_{spr}}{A_{450}}$, the error should lie in the absolute level of both $A_{450}$ and $A_{spr}$, possibly an offset of both absorption values.
- Underestimating the range of the interparticle potential:
  As noted in eq (5), the repulsive EDL potential decays exponentially with the inverse of the Debye length and, as stated in eq. (6), the inverse of the Debye length increases with ionic strength ($\kappa \propto \sqrt{I}$). As noted in section 3.5, the citrate solution is assumed to dissociate completely, thereby likely overestimating the ionic strength.

Theoretically, overestimating the repulsive interactions between AuNP and the substrate would also result in a too low AuNP number density. However, as only eq. (10) is used in the model to model the particle-substrate interaction, there should be no impact from overestimating the repulsive interactions between AuNP and the substrate.

# 5 CONCLUSIONS

Of the functionalisation methods tested in this thesis, silanisation with UV/$O_3$ pre-treatment seems like the best alternative for creating AuNP number density gradients on polystyrene substrates. The method exhibited AuNP number density of same order of magnitude as on the glass reference samples ($5.73 \cdot 10^{14}$ $m^{-2}$, compared to $2.48 \cdot 10^{15}$ $m^{-2}$ for the glass reference) and similar range of dispersion (75 nm, compared to 40-60 nm for the glass reference), indicating that repulsive interparticle forces determine the interparticle distance – which is crucial for creating AuNP number density gradients. It should, however, be noted that these conclusions are based on few experiments and need to be verified by additional (repeated) experiments.

The rudimental computational model seems to capture the basic phenomena of AuNP adsorption but underestimates the AuNP number density and the interparticle potential (or at least the range of the interparticle potential). There are several likely causes for these errors, e.g. underestimating the bulk concentration of AuNPs (experimental error) or overestimating the ionic strength of the solution (due to the model assuming complete dissociation of the citrate buffer).

# 6 FURTHER WORK

As the work presented in this thesis outlines a first step towards creating AuNP number density gradients on polystyrene substrates, there is plenty of interesting work left for the future. Some suggestions for topics of future work are listed in the sections below.

## 6.1 ADDITIONAL EXPERIMENTS TO VERIFY RESULTS

A reasonable first step for future work would be to verify the results by repeating the experiments. Of special interest would be confirming the most promising results:

- Silanisation, with UV/$O_3$ as pre-treatment
- Poly-l-lysine, with $O_2$ plasma as pre-treatment

Furthermore, it would be interesting to repeat the test on untreated polystyrene to confirm that the high AuNP number density was indeed due to an experimental error.

It would also be of interest to investigate the surface chemistry of the polystyrene substrates after the respective pre-treatments (e.g. UV/$O_3$ and $O_2$ plasma) to investigate what functional groups were introduced by the pre-treatments (as hypothesised in section 4.3). This could be done by e.g. x-ray photoelectron spectroscopy (XPS). By investigating the surface chemistry also after silanisation and coating with poly-l-lysine, it could be possible to gain insight on what is limiting the AuNP deposition, e.g. if the UV/$O_3$ treatment is creating too few hydroxyl groups on the polystyrene surface so that the surface can only be silanised to a low extent.

## 6.2 TESTING AUNP GRADIENT APPLICATION ON POLYSTYRENE SUBSTRATES

The scope of this report was to investigate uniform AuNP deposition on polystyrene substrates, with the goal of showing that some functionalisation method(s) can achieve similar AuNP number density on polystyrene substrates as on glass substrates. As the final product requires a number density gradient of AuNPs, that is, AuNPs of non-uniform distribution, an interesting next step would be to try creating gradients on functionalised polystyrene substrates.

For this work, the goal is reasonably that the entire gradient – not only at the densest region – should be similar between the functionalised polystyrene substrate and the glass substrate. To achieve this, the method of creating gradients might need to be optimised for the functionalised polystyrene substrates.

## 6.3 INVESTIGATING CYTOCOMPATIBILITY OF THE FUNCTIONALISATION METHOD(S)

As the application of the AuNP number density gradients lies within cell studies, e.g. studying stem cell differentiation, the cytocompatibility of the functionalisation method is crucial (although not within the scope of this master thesis). Some insights to the cytocompatibility should be possible to gain from investigating the surface chemistry of the substrates after functionalisation (see section 6.1). To gain more insights, *in vitro* cell cultivation studies could be performed on the functionalised substrates. Furthermore, if surface roughness is critical for the cytocompatibility, the functionalised substrates could be investigated by atomic force microscopy (AFM) to understand if the functionalisation methods, especially some of the pre-treatments to oxidise the polystyrene surface, has increased the surface roughness too much.

## 6.4 IMPROVING THE COMPUTATIONAL MODEL FOR AUNP ADSORPTION

To improve the rudimental computational model of the AuNP adsorption, several of the assumptions in the model should be reviewed. As mentioned, the assumption of complete dissociation of the citrate ions should be reviewed to better model the ionic strength of the solution to investigate if it improves the size and/or range of the interparticle potential. Furthermore, some parameters in the existing model are approximated with values for water, so parameter values better representing the citrate solution should be sought.

Additionally, the computational model of AuNP adsorption in this thesis was developed for uniform AuNP deposition on the substrate surface. When gradient AuNP deposition (non-uniform AuNP distribution) is tested, the model should be extended to account for a transient adsorption process. Moreover, modelling the gradient AuNP deposition depends on modelling a varying ionic strength, so a better approximation of the ionic strength is crucial also for this case.

# REFERENCES


[1] M. J. Evans and M. H. Kaufman, "Establishment in Culture of Pluripotential Cells from Mouse Embryos," *Nature,* vol. 292, pp. 154-156, 1981.

[2] J. A. Thomson , J. Itskovitz-Eldor, S. S. Shapiro, M. A. Waknitz, J. J. Swiergiel, V. S. Marshall and J. M. Jones, "Embryonic Stem Cell Lines Derived from Human Blastocysts," *Science,* vol. 282, no. 5391, pp. 1145-1147, 1998.

[3] M. Mimeault and S. K. Batra, "Concise Review: Recent Advances on the Significance of Stem Cells in Tissue Regeneration and Cancer Therapies," *Stem Cells,* vol. 24, no. 11, pp. 2319-2345, 2006.

[4] K.-M. Chan, S. P. Raikwar and N. Zavazava, "Strategies for Differentiating Embryonic Stem Cells (ESC) into Insulin-Producing Cells and Development of Non-Invasive Imaging Techniques Using Bioluminescence," *Immunol Res,* vol. 39, pp. 261-270, 2007.

[5] I. Klimanskaya, N. Rosenthal and R. Lanza, "Derive and Conquer: Sourcing and Differentiating Stem Cells for Therapeutic Applications," *Nature Rewiews Drug Discovery,* vol. 7, pp. 131-142, 2008.

[6] M. T. Mitjavila-Garcia, C. Simonin and M. Peschanski, "Embryonic Stem Cells: Meeting the Needs for Cell Therapy," *Advanced Drug Delivery Reviews,* vol. 57, pp. 1935-1943, 2005.

[7] A. Lundgren, M. Hulander, J. Brorsson, M. Hermansson, H. Elwing, O. Andersson, B. Liedberg and M. Berglin, "Gold-Nanoparticle-Assisted Self-Assembly of Chemical Gradients with Tunable Sub-50 nm Molecular Domains," *Particle & Particle Systems Characterization,* vol. 31, pp. 209-218, 2014.

[8] M. Peixoto de Almeida, E. Pereira, P. Baptista, I. Gomes, S. Figueiredo, L. Soares and R. Franco, "Gold Nanoparticles as (Bio)Chemical Sensors," in *Comprehensive Analytical Chemistry*, Amsterdam, Elsevier, 2014, pp. 529-567.

[9] Y. Xia and N. J. Halas, "Shape-Controlled Synthesis and Surface Plasmonic Properties of Metallic Nanostructures," *Materials Research Society Bulletin,* vol. 30, no. 5, pp. 338-348, 2005.

[10] E. Cottancin, G. Celep, J. Lermé, M. Pellarin, J. R. Huntzinger, J. L. Vialle and M. Broyer, "Optical Properties of Noble Metal Clusters as a Function of the Size: Comparison between Experiments and a Semi-Quantal Theory," *Theoretical Chemical Accounts,* vol. 116, pp. 514-523, 2006.

[11] S. Kumar Ghosh, "Spectroscopic Evaluation of 4-(dimethylamino)pyridine versus Citrate as Stabilizing Ligand for Gold Nanoparticles," *Colloids and Surfaces A: Physicochemical and Engineering Aspects,* vol. 371, no. 1-3, pp. 98-103, 2010.

[12] P. K. Jain, K.-S. Lee, I. H. El-Sayed and M. A. El-Sayed, "Calculated Absorption and Scattering Properties of Gold Nanoparticles of Different Size, Shape, and Composition: Applications in Biological Imaging and Biomedicine," *The Journal of Physical Chemistry B,* vol. 110, no. 14, pp. 7238-7248, 2006.

[13] W. Haiss, N. T. K. Thanh, J. Aveyard and D. G. Fernig, "Determination of Size and Concentration of Gold Nanoparticles from UV-Vis Spectra," *Analytical Chemistry,* vol. 79, pp. 4215-4221, 2007.

[14] J. Turkevich, P. Cooper Stevenson and J. Hillier, "A Study of the Nucleation and Growth Processes in the Synthesis of Colloidal Gold," *Discussions of the Faraday Society,* vol. 11, pp. 55-75, 1951.

[15] A. M. Alkilany, S. R. Abulateefeh, K. K. Mills, A. I. Bani Yaseen, M. A. Hamaly, H. S. Alkhatib, K. M. Aiedeh and J. W. Stone, "Colloidal Stability of Citrate and Mercaptoacetic Acid Capped Gold Nanoparticles Upon Lyophilization: Effect of Capping Ligand Attachment and Type of Cryoprotectants," *Langmuir,* vol. 30, pp. 13799-13808, 2014.

[16] D. P. Stankus, S. E. Lohse, J. E. Hutchison and J. A. Nason, "Interactions between Natural Organic Matter and Gold Nanoparticles," *Environmental Science & Technology,* vol. 45, pp. 3238-3244, 2011.

[17] R. Ghosh, J. Deka, A. Chattopadhyay and A. Paul, "Conformation Aspect in the α-Amylase Induced Agglomeration of Citrate-Stabilized Gold Nanoparticles," *RSC Advances,* vol. 3, pp. 23015-23027, 2013.

[18] L. Zhao, D. Jiang, Y. Cai, X. Ji, R. Xie and W. Yang, "Tuning the Size of Gold Nanoparticles in the Citrate Reduction by Chloride Ions," *Nanoscale,* vol. 4, pp. 5071-5076, 2012.

[19] F. Soares Lamerias, A. Leles de Souza, V. Alves Rodrigues de Melo, E. Henrique Martins Nunes and I. Dionizio Braga, "Measurement of the Zeta Potential of Planar Surfaces with a Rotating Disk," *Materials Research,* vol. 11, no. 2, pp. 217-219, 2008.

[20] C. R. Vistas, A. C. P. Águas and G. N. M. Ferreira, "Silanization of Glass Chips — A Factorial Approach for Optimization," *Applied Surface Science,* vol. 286, pp. 314-318, 2013.

[21] D. Zhang, S. M. Dougal and M. S. Yeganeh, "Effects of UV Irradiation and Plasma Treatment on a Polystyrene Surface Studied by IR-Visible Sum Frequency Generation Spectroscopy," *Langmuir,* vol. 16, pp. 4528-4532, 2000.

[22] P. Yang and W. Yang, "Hydroxylation of Organic Polymer Surface: Method and Application," *ACS Applier Materials & Interfaces,* vol. 6, pp. 3759-3770, 2014.

[23] M. Bernmalm, "Substrate Independent Adsorption of Gold Nanoparticles by Using Polypeptides as Adhesive," Chalmers Univerity of Technology, Gothenburg, 2013.

[24] J. Eklöf, T. Gschneidtner, S. Lara-Avila, K. Nygård and K. Moth-Poulsen, "Controlling Deposition of Nanoparticles by Tuning Surface Charge of SiO2 by Surface Modifications," *RCS Advances,* vol. 6, pp. 104246-104253, 2016.

[25] J. N. Israelachvili, "Van der Waals Forces between Particles and Surfaces," in *Intermolecular and Surface Forces*, Amsterdam, Elsevier, 2011, pp. 253-289.

[26] J. N. Israelachvili, "Electrostatic Forces between Surfaces in Liquids," in *Intermolecular and Surface Forces*, Amsterdam, Elsevier, 2011, pp. 291-340.

[27] R. D. Handy, F. von der Kammer, J. R. Lead, M. Hassellöv, R. Owen and M. Crane, "The Ecotoxicology and Chemistry of Manufactured Nanoparticles," *Ecotoxicology,* vol. 17, pp. 287-314, 2008.

[28] M. Bartelt and V. Privman, "Kinetics of Irreversible Monolayer and Multilayer Adsorption," *International Journal of Modern Physics B,* vol. 5, no. 18, pp. 2883-2907, 1991.

[29] N. I. Lebkowa, "Aggregation of Charged Colloidal Particles," in *Polyelectrolyte Complexes in the Dispersed and Solid State I*, Berlin, Heidelberg, Springer, 2012, pp. 57-96.

[30] K. Park, H. Park and R. M. Albrecht, in *Colloidal Gold Principles, Methods and Applications*, San Diego, Academic Press, 1989, pp. 489-518.

[31] R. R. Bhat, D. A. Fischer and J. Genzer, "Fabricating Planar Nanoparticle Assemblies with Number Density Gradients," *Langmuir,* vol. 18, pp. 5640-5643, 2002.

[32] B. D. Ripley, “Modelling Spatial Patterns,” *Journal of the Royal Statistical Society Series B Statistical Methodology,* vol. 39, pp. 172-192, 1977.